A Late glacial-early Holocene multiproxy record, Fram Strait, Polar North Atlantic

S. Aagaard-Sørensen[1*], K. Husum[1], M. Hald[1], T. Marchitto[2], K. Werner[3] and R. Spielhagen[3,4]

[1] Department of Geology, University of Tromsø, 9037 Tromsø, Norway;

[2] Department of Geological Sciences and Institute of Arctic and Alpine Research, University of Colorado, Campus Box 450, Boulder, Colorado 80309, USA

[3] Leibniz Institute of Marine Sciences IFM-GEOMAR, Wischhofstraße 1-3, D-24148 Kiel, Germany

[4] Academy of Sciences, Humanities, and Literature, 53151 Mainz, Germany

[*]Author for correspondence: (e-mail: Steffen.Sorensen@uit.no)

Abstract

Paleoceanographic changes have been studied in the eastern Fram Strait during the Late Glacial – Early Holocene transition based on a sediment core from 1488 meters water depth (78˚54 N). This core site is situated close to the Arctic Front under the modern day axis of Atlantic Water inflow from the Nordic Seas towards the Arctic Ocean. The age model is constrained by four accelerator mass spectrometry (AMS) ^{14}C dates. Planktic foraminiferal assemblages were analyzed using the >100µm size fraction, foraminiferal δ^{13}C and δ^{18}O stable isotopes were measured on the polar planktic foraminifer *Neogloboquadrina pachyderma* and physical and chemical analyses have been carried out on the bulk sediment samples. Furthermore Mg/Ca-ratios were measured on *N. pachyderma*. This is the first time this method has been tested in a late Glacial – early Holocene high Arctic paleoceanographic setting. The method provides valuable information of the subsurface temperature variability and in conjunction with the stable isotope measurements also the subsurface salinity variability. The Sea Surface Temperature ($SST_{Mg/Ca}$) and Sea Surface Salinity (SSS) reconstructions show values fluctuating between 1.9 to 5.5°C and 33.6 to 35.2, respectively. The results are used in combination with the other investigated well established proxies to interpret the paleoenvironmental development. From 14,000 to 10,300 cal yr B.P. cold polar sea surface conditions existed and *N. pachyderma* dominated the planktic fauna. The period had extensive sea ice cover, iceberg transport and low surface temperatures resulting in low primary production. Atlantic Water inflow was reduced compared with the present day, but

existed as a subsurface current. At ca. 10,500 cal yr B.P. Atlantic Water inflow increased and the Arctic Front retreated westward resulting in a large surface water temperature increase of ca. 5°C reflected by the shift in overall faunal composition where the subpolar planktic foraminifer *Turborotalita quinqueloba* became dominant. Warm conditions prevailed in the uppermost water column until 8,600 cal yr B.P. The period had strong influence from Atlantic Water at the surface indicated by high sea surface temperatures, high foraminiferal fluxes, increased primary productivity and a near absence of ice rafted debris. Subsurface inflow of Atlantic Water continued with modest temperature change compared to previous period.

1. Introduction

The Arctic region reacts and has reacted strongly to modern and past global climate change (e.g. IPCC, 2007; Hald et al., 2007). One of the major components controlling the modern Arctic environment is influx and volume of relatively warm and saline Atlantic Water flowing northwards into the Arctic Ocean (Schauer et al., 2004). This influx primarily takes place through two gateways: the deep Fram Strait (Schauer et al., 2004) and the shallower Barents Sea (Schauer et al., 2002). In order to enhance the understanding of future climate changes in the Arctic region it is a prerequisite to understand and quantify past rapid oceanic changes. Developing a precise temperature proxy in Arctic and Polar oceanic environments has proven difficult. Reconstructions of sea surface water temperatures using transfer functions are encumbered by the low faunal diversity in the Arctic (e.g. Pflaumann et al., 2003). Stable isotopes measured on foraminiferal calcareous tests reflect salinity, temperature, and degree of ventilation of the ambient water masses (e.g. Spielhagen and Erlenkeuser, 1994). Mg/Ca ratios of foraminifers reflect water temperatures during shell growth and have been shown to allow temperature reconstructions for T >2.5°C (Kozdon et al., 2009). This study aims to test measurements of Mg/Ca-ratios as an Arctic temperature proxy investigating the transition from the cold late Glacial and into the warm early Holocene period in the Fram Strait. In a recent study Spielhagen et al. (2011) utilize the Mg/Ca method, alongside the SIMMAX modern analog technique (Pflaumann et al., 1996), to resolve a significant SST increase over the past ca. 150 years in the eastern Fram Strait. Previous studies of the spatial and temporal oceanographic evolution in the Fram Strait show rapid changes through late Glacial – early Holocene transition. Atlantic Water masses were advected into the area during the Bølling-Allerød interstadial (Ślubowska-Woldengen et al., 2005, 2007; Ebbesen et al., 2007; Rasmussen, T. L. et al., 2007). During the Younger Dryas

stadial the water masses remained as a submerged water mass under a layer of polar surface water (Rasmussen, T. L. et al., 2007). During the early Holocene advection of Atlantic Water was strong and dominated the upper water column (Hald et al., 2007). The investigated sediment core is situated under the axis of present day inflow of Atlantic Water close to the Arctic Front dividing Atlantic and Arctic water masses. This multiproxy study includes planktic foraminiferal fauna analyses, planktic stable isotopes ($\delta^{18}O$ and $\delta^{13}C$) and Mg/Ca ratios which have been used to reconstruct sea surface temperatures (SST) and salinities (SSS).

2. Oceanographic setting

The Fram Strait is a 2600 m deep passage situated between Svalbard and Greenland that connects the Greenland and Norwegian Sea to the Arctic Ocean (Fig 1). The surface waters in the Fram Strait are dominated by two contrasting water masses separated by a transition zone termed the Arctic Front (Swift, 1986). Atlantic Water is transported towards the Arctic Ocean via the West Spitsbergen Current, the meriodional branch of the North Atlantic Current (Loeng et al., 1997; Schauer et al., 2002) (Fig 1). The West Spitsbergen Current is topographically steered along the western slope of Spitsbergen through the eastern Fram Strait and into the Arctic Ocean (Blindheim and Rey, 2004; Walczowski et al., 2005). The West Spitsbergen Current carries warm and saline Atlantic Water (T: 3 to 7°C; S: 34.9 to 35.2) northward and occupies the upper 500 to 700 m of the water column below a ca. 25 m thick mixed layer in the eastern part of the Fram Strait (Fig 2) (Schauer et al., 2004; Walczowski et al., 2005). This makes the eastern Fram Strait the main pathway for heat and salt advection into the Arctic Ocean (Schauer & Beszczynska-Möller, 2009). In the western part of the Fram Strait the East Greenland Current occupies the upper ca. 150 m of the water column carrying a cold, low salinity (T: 0 to -1.7°C; S: ca. 30 to 34) polar water mass southward (Woodgate et al., 1999; Rudels et al., 2005) (Fig 1). The East Greenland Current furthermore carries most (>90%) of the sea ice exported from the Arctic Ocean (Woodgate et al., 1999; Rudels et al., 1999; 2005). At ca. 78°N the advected Atlantic Water submerges (e.g., Aagaard and Carmack, 1989) and a major part re-circulates in the Fram Strait creating a southward return flow, the Return Atlantic Water (RAW) (T: >0°C; S: >34.90), below the East Greenland Current (Bourke et al., 1988) (Fig 1). North of Svalbard Atlantic Water continues as a subsurface current into the Arctic Ocean northward as the Yermak Slope Current (Manley, 1995) and eastward as the Svalbard Branch along the northern continental slope of Svalbard (Aagaard et al., 1987; Manley, 1995) (Fig 1). In the Arctic Ocean the warm

Atlantic Water of the Yermak Slope Current and Svalbard Branch mixes with Polar Water forming Arctic Water. Part of Arctic Water of the Svalbard Branch enters the north-eastern Barents Sea becoming the south-westward flowing East Spitsbergen Current (Skogseth et al., 2005) (Fig 1).

3. Material and methods

Kastenlot core MSM05/5-712-2 was retrieved from 1488 m water depth in the Fram Strait (78˚56 N, 06˚46 E) during a cruise with RV "Maria S. Merian" in August 2007 (Fig 1). Conductivity, temperature, and depth were measured prior to coring (Fig 2). Proxy data from the 8.94 m long sediment core are presented here at the core depth interval from 209 to 441cm (Fig 3). The interval is constrained by four accelerator mass spectrometry (AMS) radiocarbon date measurements performed at the Leibniz Laboratory of Kiel University, Germany and Poznań Radiocarbon Laboratory, Poland (Fig 3, Table 1). Radiocarbon dating was performed on planktic foraminifer (*Neogloboquadrina pachyderma*) (Table 1). Calibration of the radiocarbon dates was performed using Calib version 6.0 (Reimer et al., 2004; Stuiver et al., 2005) and the marine calibration curve Marine09 (Hughen et al., 2004; Reimer et al., 2009) (Table 1). A total reservoir age of 551±51 was used. This value was reached using the standard reservoir correction of 400 years and the modern reservoir age (ΔR) of 151 ± 51 from the nearby Magdalenefjorden (Mangerud and Gulliksen, 1975; Mangerud et al., 2006). The age model was established by linear interpolation between the calibrated radiocarbon dates using the mean of the 2σ interval of highest probability as individual tie points (Fig 3, Table 1). In figures and text all dates will refer to calibrated years before present, B.P. (1950). The Late Glacial - Holocene chronostratigraphical zones mentioned in the text and used on figures are based on the most recent divisions defined on the basis of Greenland ice cores (Rasmussen, S.O. et al., 2006; Rasmussen, S.O. et al., 2007; Steffensen et al., 2008; Walker et al., 2009): Bølling-Allerød interstadial 14,650 to 12,850 cal yr B.P., Younger Dryas 12,850 to 11,650 cal yr B.P. and Holocene 11,650 cal yr B.P. to present.

The lithology of the sediment core was visually described onboard after the coring (Fig 4). Samples at 6 cm-intervals were freeze-dried and wet sieved through the 63 µm, 100 µm and 1 mm sieves. Grain size distribution was determined by weighing the resulting fractions at 63-100 µm, 100 µm-1 mm and >1 mm. The >1 mm size fraction is considered as ice rafted debris (IRD) (Fig 4). Total organic carbon (TOC) and total carbon (TC) were measured at 6

cm-intervals at 209 to 298 cm and at 3 cm-intervals at 298 to 341 cm (Fig 4). TC and TOC were measured using a Leco CS 200 furnace at the University of Tromsø. The TC content (wt.%) was measured directly on bulk sediment samples while the TOC content (wt.%) was measured on samples pre-treated with HCl (10%) to remove $CaCO_3$ before combustion (1350ºC). The $CaCO_3$ content (wt.%) was calculated using the equation: $CaCO_3$ = (TC-TOC)*100/12 (e.g. Knies et al., 2003) (Fig 4).

The same samples were used to analyse the planktic foraminiferal distribution. Approximately 300 planktic specimens of the 100-1000 µm size fraction were identified to species level, and the relative distribution together with the fluxes were calculated (Fig 5). The sea surface temperatures ($SST_{Transfer}$) were reconstructed using transfer functions utilizing the computer program C.2 version 1.3 (Juggins, 2002). The transfer functions used to reconstruct $SST_{Transfer}$ included Weighted Average Partial Least Square (WAPLS), Maximum Likelihood Method (ML) and the Modern Analogue Technique (MAT) (Telford et al., 2004; Telford and Birks, 2005) (Fig 5). The modern foraminiferal training set applied in the reconstructions is based on planktic specimens (>150 µm size fraction) from core top samples in the Atlantic Ocean (60°S to 90°N) covering large variations of sea surface temperatures at 10 m water depth (Pflaumann et al., 2003).

Stable isotope measurements were performed at the Leibniz-Laboratory for Radiometric Dating and Stable Isotope Research, Kiel using a Finnigan MAT 251 mass spectrometer (reproducibility of ±0.03‰ for $\delta^{13}C$ and ±0.06‰ for $\delta^{18}O$) (Fig 6). Stable oxygen and carbon isotopic ratios were measured on 20 to 30 tests of the planktic foraminifer species *N. pachyderma* with an average size of 150 to 200 µm. All measurements were calibrated to Pee Dee Belemnite (PDB) standard. Measurements were carried out at 1 cm-intervals apart from at 373-380 cm core depth where scarcity of foraminiferal fauna prevented analysis. A vital effect of 2.1‰ representative for the Arctic Ocean has been added to the $\delta^{13}C$ values (Volkmann and Mensch, 2001). The $\delta^{18}O$ isotope record was not corrected for vital effects (Jonkers et al., 2010) but for the ice volume effect (Fairbanks, 1989).

Trace element analysis was performed every 3 cm on an average of 50 *N. pachyderma* tests (Fig 7). The tests were picked from the size fraction 150-212 µm in order to minimize possible size-dependent bias (Elderfield et al., 2002). Foraminiferal tests were gently crushed between glass plates to expose all test chambers to the reductive (anhydrous hydrazine) and oxidative (H_2O_2) cleaning procedures following Boyle and Keigwin (1985) and Boyle and

Rosenthal (1996). Cleaned samples were analyzed for Mg/Ca, Mn/Ca and Fe/Ca by magnetic-sector singlecollector ICP-MS, on a Thermo-Finnigan Element2 at the Litmann laboratory, University of Colorado (Fig 7). Replicate analysis was performed for every ca. 20. sample. The average Mg/Ca reproducibility of sample splits was ±0.049 mmol/mol (n=3) which is below 4% difference between the average and recorded duplicate values (Fig 7). The system has long-term 1σ precisions for Mg/Ca of 0.54% (Marchitto, 2006). Samples with >100 µmol/mol in regards to Fe/Ca (n=3) and Mn/Ca (n=4) were omitted due to possible contamination by detrital material or secondary diagenetic coatings, which could lead to biased Mg/Ca values (Barker et al., 2003). One additional data point at 395-394 cm core depth was omitted due to a combination of very high Mg/Ca and $\delta^{18}O$ values generating a combined effect of unrealistically high calculated salinity values (Fig 7).

3.1 SST and SSS calculations based on $\delta^{18}O$ and Mg/Ca ratios

Quantitative reconstructions of sea surface temperatures (SST) were obtained using measured $\delta^{18}O$ and Mg/Ca values and transfer functions (Fig 8). Sea surface temperatures were calculated from measured $\delta^{18}O$ values ($SST_{Isotope}$) using the equation of Shackleton (1974):

(Eq.1) $T\ (°C) = 16.9 - 4*(\delta^{18}O_{foraminifer,\ vs.\ V\text{-}PDB} + \delta^{18}O_{vital\ effect,\ vs.\ V\text{-}PDB} - \delta^{18}O_{water,\ vs.\ V\text{-}SMOW})$,

where $\delta^{18}O_{water}$ is standard mean ocean water composition (V-SMOW). Conversion from the Standard Mean Ocean Water (SMOW) scale to calcite on the PeeDee Beleminte (PBD) scale was done by subtracting 0.2‰ (Shackleton, 1974). For tentative temperature calculations a constant value of 0.3‰ PDB for paleo-$\delta^{18}O_{water}$ was used. This value corresponds to the average modern value on the West Spitsbergen margin at 25-500 m water depth (Meredith et al., 2001). The measured Mg/Ca elemental ratios were converted into temperatures ($SST_{Mg/Ca}$) by using the species-specific (*N. pachyderma*) linear equation of Kozdon et al. (2009):

(Eq. 2) $Mg/Ca\ (mmol/mol) = 0.13*T + 0.35$.

Despite exponential thermodynamic control on Mg uptake in calcareous foraminiferal tests this equation assumes that linearity adequately depicts the Mg uptake/temperature relation in the narrow temperature range inhabited by *N. pachyderma* (Kozdon et al., 2009). The equation is based on cross calibrated Mg/Ca and $\delta^{44/40}Ca$ proxy signals of *N. pachyderma* in Holocene core top samples from the Nordic Seas and works well for reconstructed temperatures above ca. 2.5°C (Mg/Ca >0.74 mmol/mol) (Kozdon et al., 2009). However,

when temperatures are lower than 2.5°C which is associated with salinities less than 34.5, the method loses its precision (Kozdon et al., 2009). Paleo $\delta^{18}O_{water, vs. V\text{-}SMOW}$ was calculated using Eq. 1 in conjunction with Eq. 2 (Fig 8). Paleo $\delta^{18}O_{water, vs. V\text{-}SMOW}$ values were translated into paleo sea surface salinity (SSS) (Fig 8) using the mixing line equation of Craig & Gordon (1965) representing the North Atlantic:

(Eq. 3) $\delta^{18}O_{water, vs. V\text{-}SMOW} = -21.2 + 0.61*SSS$.

4. Results

The sediment comprises two different lithological units. Unit B at ca. 14,000 to 10,300 cal yr B.P. (442 – 323 cm) holds dark olive grey monosulphide-rich silty clay with ca. 1 cm thick olive black laminations. The overlying unit A at ca. 10,300 to 8,600 cal yr B.P. (323 – 208 cm) holds dark homogenous olive grey, monosulphide-rich bioturbated silty clay (Fig 4). The sediment accumulation rate of unit B is 32 cm/kyr and 59 to 108 cm/kyr in unit A (Fig 3). Unit B holds 2 to 7 wt.% material >63 µm and up to 4 wt.% material >1 mm (IRD). Two periods at 13,300 to 12,200 and 11,500 to 10,900 cal yr B.P. hold higher concentrations of material >1mm averaging 2 wt.% (Fig 4). Unit A is very fine grained with 98 wt.% of material <63 µm (Fig 4). A diatom rich layer was identified at 10,500 to 9,800 cal yr B.P. (329 – 281 cm) (Fig 4). The concentrations of total organic carbon (TOC) and total carbon (TC) in the sediment concurrently increase at ca. 11,500 cal yr B.P. from averages between ca. 0.8 and 1.2 wt.% and ca. 1.3 to 1.7 wt.%, respectively (Fig 4). The TC signal exhibit a second increase at ca. 10,000 cal yr B.P. followed by a steady increase. The TOC signal exhibits a maximum at 11,400 to 10,300 cal yr B.P. followed by a sustained decline throughout the remaining interval. The resultant $CaCO_3$ signal exhibits low values averaging 4.5 wt.% prior to 10,000 cal yr B.P. followed by a distinct increase from ca. 5 to 13 wt.% during the succeeding 1400 years (Fig 4).

Foraminiferal analyses show a good preservation of the planktic foraminiferal fauna as minimal or no signs of test dissolution were observed. Polar *N. pachyderma* and subpolar *T. quinqueloba* dominate the planktic foraminiferal fauna (Fig 5). The clear dominance of these the two species is characteristic for Arctic marine environments (e.g. Johannessen et al., 1994; Carstens et al., 1997; Volkmann, 2000). The planktic faunal distribution pattern (Fig 5) at 14,000 to 10,500 cal yr B.P. shows a low total faunal flux (ca. 2 specimens/cm^2*yr) dominated by *N. pachyderma* (>86%) with *T. quinqueloba* and *Neogloboquadrina incompta* (Darling et al., 2006) as secondary species (<10%). Between 10,500 and 10,100 cal yr B.P. *T.*

quinqueloba becomes the dominant species coincident with increasing planktic fluxes (Fig 5). Relative abundance of *T. quinqueloba* averages 63% from 10,100 to 8,600 cal yr B.P. while overall planktic fluxes remain high averaging 50 specimens/cm^2*yr (Fig 5). The faunal diversity increases during this period with additional species such as *Globigerina bulloides* (>3.1%), *Globigerinita calida* (>2.4%), *Globigerinita glutinata* (>2.2%) and *Globigerinita uvula* (up to ca. 10%). *N. pachyderma* only constitutes ca. 25% and *N. incompta* ca. 6% of the total planktic foraminiferal distribution. *Globigerinita uvula* is primarily found from 10,000 to 9,200 cal yr B.P. with a peak in relative abundance of ca. 10% at 9,900 cal yr B.P. (Fig 5). One data point at 8,800 cal yr B.P. breaks the dominance of *T. quinqueloba* with abundance of *N. pachyderma* reaching 68% coincident with markedly lowered overall planktic flux (Fig 5).

The sea surface temperatures obtained by transfer functions ($SST_{Transfer}$) show low temperatures ranging from 2 to 4°C prior to ca. 10,500 cal yr B.P. A rapid temperature increase occurs from ca. 10,500 to 10,100 cal yr B.P. followed by relatively high temperatures, 7 to 9°C from 10,100 to 8,600 cal yr B.P. (Fig 5). The WALPS method indicates early maximum temperatures followed by a slow decline, while the MAT and ML methods show relatively stable (ca. 9°C) temperatures. All three reconstruction methods reflect the faunal dominance shift at 8,800 cal yr B.P. as a pronounced cooling event (Fig 5). The uncertainty of the temperature reconstructions, the root mean squared error of prediction (RMSEP), is about 1.9ºC for WALPS, 1.2ºC for MAT and 1.8ºC for ML. The RMSEP is often used to evaluate and select the transfer function model with most predictive power (i.e. yielding the best temperature estimate), but it suffers from bias by possible spatial autocorrelation in the training set causing overoptimistic estimates of the RMSEP (Telford and Birks, 2005). This bias is most pronounced for MAT and decreases progressively for WALPS and ML (Telford and Birks, 2005). The ML based SST reconstruction is therefore chosen as the best representative for the present record. However, the $SST_{Transfer}$ reconstructions may be ca. 1 to 2°C too low for colder temperatures (< 4°C) due to the difference between the size fraction of the paleo fauna (> 100µm) and the training set (>150µm) (Hald et al., 2007).

The $\delta^{13}C$ values show two local maxima at ca. 12,700 (2.35‰) and ca. 8,800 cal yr B.P. (2.55‰) in addition to a broad maximum at 11,600 to 10,200 cal yr B.P. (ca. 2.35‰). Minimum values are seen at ca. 12,400 (2.1‰), 11,650 (2.2‰) and at 10,200 to 9,000 cal yr B.P. (ca. 2.2‰) (Fig 6).

The $\delta^{18}O$ values show relatively high values of 3.2‰ at ca. 13,000 cal yr BP which increases to 3.7‰ at 12,100 cal yr B.P. (Fig 6). Low values (around 2.9‰) at 11,900 to 11,500 cal yr B.P. are followed by a 0.6‰ increase leading to a maximum at ca. 11,400 to 11,200 cal yr B.P. (ca. 3.5‰). From ca. 11,000 cal yr B.P. the values decline and reach a minimum at ca. 9,500 cal yr B.P. (ca. 2.5‰) with one marked excursion towards heavier values at ca. 10.000 cal yr B.P. A slightly increasing trend is observed after 9,500 cal yr B.P. (Fig 6).

The Mg/Ca ratios show values from ca. 0.6 to 1.07 mmol/mol throughout the analysed interval. An overall slightly increasing trend is noticed towards the youngest part of the record (Fig 7). Maximum values are found at ca. 13,200, ca. 11,600 and ca. 9,800 cal yr B.P. Minima are found at ca. 12,200 and ca. 11,000 cal yr B.P. The Mg/Ca values exhibit a minor change with average values of 0.81 mmol/mol prior to and 0.86 mmol/mol after 10,300 cal yr B.P. The Fe/Ca ratio generally has values of 10 to 50 µmol/mol throughout the record while the Mn/Ca ratios average 40 µmol/mol prior to and 70 µmol/mol after 10,500 cal yr B.P. (Fig 7).

4.1 SST and SSS calculations based on $\delta^{18}O$ and Mg/Ca ratios

Sea surface temperatures based on Mg/Ca ratios ($SST_{Mg/Ca}$) show relatively moderate temperature fluctuations between ca. 3 and 5°C throughout the record. Temperature maxima are recorded at ca. 13,200, ca. 11,600 and ca. 9,800 cal yr B.P. Average temperatures are 3.6ºC before and 4.0ºC after 10,300 cal yr B.P. (Fig 7).

Sea surface temperatures based on $\delta^{18}O$ ($SST_{Isotope}$) are calculated assuming a constant salinity of 35 (Fig 8). The $SST_{Isotope}$ values fluctuate between ca. 4 to 8°C.

In order to calculate sea surface salinity (SSS), various relevant vital effects (Volkmann and Mensch, 2001; Nyland et al., 2006; Jonkers et al., 2010) and mixing line equations (Craig & Gordon, 1965; Östlund et al., 1987; Simstich et al., 2003) were tested. Estimates were disregarded if they were higher than 35.2, the modern value at the core site (Fig 2). The $\delta^{18}O$ vital effects proposed by Volkmann and Mensch (2001) (1.3‰) and Nyland et al. (2006) (0.6‰) resulted in unrealistically high SSS estimates (>35.2) regardless of Mg/Ca and mixing line equation selected. The $SST_{Mg/Ca}$ values combined with $\delta^{18}O$ vital effect corrected according to Jonkers et al. (2009) constantly produce SSS values below 35.2. However, the SSS estimates differ in their overall variability and generated salinity minima, depending on the choice of the mixing line equation. The mixing line equation of Craig & Gordon (1965)

(Eq. 3) representing the North Atlantic was chosen as the best representative for the present record because the reconstructed salinities stayed within the accepted range (ca. 33.5 to 35.2) (Fig 8). The reconstructed salinities reveal an overall decreasing trend showing that recorded salinities were higher during the Late Glacial than during the early Holocene (Fig 8).

5. Discussion

In the present study sea surface temperatures ($SST_{Transfer,}$ $SST_{Isotope}$ and $SST_{Mg/Ca}$) have been quantified using different proxies with a decadal to centennial resolution (Fig 8). The overall trend of the different SST reconstructions is the same, except from ca. 10,500 cal yr B.P. where $SST_{Transfer}$ increases dramatically compared to the other SST reconstructions (Fig. 8). The $SST_{Mg/Ca}$ temperature range is relatively narrow (2 to ca. 6°C) compared to the other reconstructions given that significant changes have been observed in the region during this transition (e.g. Koç et al., 2002; Rasmussen, S. O. et al., 2006; Hald et al., 2007; Rasmussen, T. L. et al., 2007; Ebbesen et al., 2007). Kozdon et al. (2009) suggest that *N. pachyderma* throughout its life cycle actively or inactively is linked to an isopycnal layer with densities (σ_t) ranging from 27.7 to 27.8. As a consequence the species prefers gradually deeper habitats with increasing temperatures, thus counterbalancing absolute sea surface temperature variations (Kozdon et al., 2009). This assumption could explain the stable signal shown by the $SST_{Mg/Ca}$ values. Furthermore, the realistic SSS values calculated on the basis of paired Mg/Ca and $\delta^{18}O$ values support the reliability of the relatively narrow temperature range (Fig 8). However, it must be emphasized that many factors are known to influence the habitat depth of planktic foraminifera including sea ice cover, proximity to sea ice margins and oceanic fronts, water column stratification, water mass distribution and food availability (Carstens et al., 1997; Volkmann, 2000; Simstich et al., 2003; Jonkers et al., 2010). Different seasonal timing of *N. pachyderma* calcification also impacts the $SST_{Mg/Ca}$ values. Jonkers et al. (2010) report largest fluxes of *N. pachyderma* during spring and in late summer when SSTs can be relatively variable. In the Arctic Ocean peak fluxes of planktic foraminifera are reported during summer at sea ice margins with high primary production (Carstens et al., 1997). Thus, during periods with prolonged sea ice cover the peak of primary production and foraminiferal calcification season, is shifted toward a warmer part of the season after commencement of sea ice breakup. In the present study the Mg/Ca-ratio values and $\delta^{18}O$ values measured in *N. pachyderma* are assumed to originate from the same depth interval and season because of the similar test sizes. The $SST_{Isotope}$ values fluctuate between ca. 4 and 8°C, which is consistently higher than the $SST_{Mg/Ca}$ (Fig 8). When *N. pachyderma* calcifies, the

uptake of the $^{18}O/^{16}O$ ratio into the test is controlled by temperature and the isotopic composition of the ambient water which largely correlates with salinity (e.g. Spielhagen and Erlenkeuser, 1994), while the Mg/Ca ratio primarily is controlled by temperature. Hence, the difference between the $SST_{Mg/Ca}$ and $SST_{Isotope}$ signals probably is due to salinity variations in the water mass. However, the salinity of the water mass varied through time. Thus, in order to reconstruct the $SST_{Isotope}$ using the $\delta^{18}O$ signal derived from *N. pachyderma* the salinity was tentatively assumed to be constant (35) (Fig 8). In the following discussion the $SST_{Isotope}$ values are only regarded as indicative while the variations in the $\delta^{18}O$ signal will be interpreted with regard to both salinity and temperature variability.

The $\delta^{13}C$ values measured on *N. pachyderma* are considered to relate to the ventilation of surface waters (Spielhagen and Erlenkeuser, 1994). High values reflect a good ventilation state with well mixed surface waters. Low values reflect less ventilated water masses possibly with increased sea ice coverage and/or presence of a melt water lid. Furthermore variation in $\delta^{13}C$ values can be linked to primary production (e.g. Katz et al., 2010). During growth phytoplankton incorporates more ^{12}C than ^{13}C. In periods of elevated phytoplankton production, ^{12}C is preferably removed from the pelagic zone leaving the remaining water mass enriched in ^{13}C. This enrichment can subsequently be recorded in planktic foraminiferal calcite as higher $\delta^{13}C$ values.

The $SST_{Transfer}$ fluctuates between ca. 2 and 5 °C prior to ca. 10,300 cal yr B.P. and average values differ only slightly from $SST_{Mg/Ca}$ (0-0.5°C) (Fig 8). After 10,300 cal yr B.P. the difference increases up to 6°C probably because $SST_{Transfer}$ reflects water temperatures at 10 m water depth while $SST_{Mg/Ca}$ records temperatures at the varying depth intervals where *N. pachyderma* preferably calcifies (Fig 8). Prior to ca. 10,300 cal yr B.P. *N. pachyderma* dominated the fauna (Fig 8) showing polar conditions (e.g. Johannsen, 1994), and IRD was relatively high indicating influence of sea ice and icebergs at the core site (Fig 4). *N. pachyderma* tend to live at shallower than 100 m water depths in areas influenced by sea ice (Volkmann, 2000; Simstich et al., 2003). The small difference between $SST_{Transfer}$ and $SST_{Mg/Ca}$ (0-0.5°C) prior to 10,300 cal yr BP could suggest a near surface habitat for *N. pachyderma* during this time. After 10,300 cal yr B.P. the dominance of the subpolar *T. quinqueloba* increased and the surface water mass warmed ca. 5°C coincidently with an IRD decrease (Fig 4, 8). We therefore assume a close vicinity of the Arctic Front (e.g. Johannessen, 1994) and less sea ice at the core site. The larger difference between $SST_{Transfer}$ and $SST_{Mg/Ca}$ after ca. 10,300 cal yr B.P. suggests that *N. pachyderma* migrated to cooler subsurface water masses (Fig 8). Essentially $SST_{Mg/Ca}$ and $SST_{Transfer}$ may record temperatures

in different parts of the water column. While $SST_{Transfer}$ always represents upper surface water masses (Pflaumann et al., 2003), the $SST_{Mg/Ca}$ records the Atlantic subsurface water layer in which *N. pachyderma* calcifies. However, the thickness of the surface layer probably varied and so did the habitat depth of *N. pachyderma*. In the following discussion it must therefore be emphasized that the water temperatures reconstructed from both methods effectively reflect temperatures at different depth intervals at different times.

5.2. Paleoenvironmental reconstruction

The paleoenvironmental reconstruction is presented in known chronostratigraphical zones in order to facilitate a direct comparison to previously published records.

5.2.1 Period: 14,000 to 12,850 cal yr B.P. (Bølling-Allerød interstadial)

In the present record the Bølling-Allerød interstadial is characterized by a planktic foraminiferal fauna assemblage dominated by *N. pachyderma* (>90%). Stable low faunal fluxes indicate that polar conditions dominated the area possibly with rare but intermittently brief sea ice free periods (Fig 5). The low faunal fluxes are mirrored by low $CaCO_3$ and TOC values indicating low overall primary production and relatively constant influx from organic matter (Fig 4). Relatively large amounts of sand (>63µm) and IRD (>1mm) shows varying influence from ice bergs and sea ice at the core site (Fig 4) while low $\delta^{13}C$ values indicate stratification which probably was caused by sea ice and melt water (Fig 6). The $SST_{Mg/Ca}$ derived from *N. pachyderma* and $SST_{Transfer}$ show similar averages of ca. 3.5°C (Fig 8). The reconstructed sea surface salinity (SSS) increased from 34.2 to 35.2 showing diminished influence from low salinity water masses throughout the Bølling-Allerød. Maximum SSS values occurred at ca. 13,100 cal yr B.P. subsequent to the maximum values of $SST_{Mg/Ca}$ indicating increased influx of Atlantic Water towards the end of the Bølling-Allerød and/or diminished melt water influence (Fig 8). Figure 9 shows paired isotope signals ($\delta^{18}O$ vs. $\delta^{13}C$) measured on *N. pachyderma* from Nordic Seas and Fram Strait water masses. The isotopic pair clustering can be used to identify and distinguish between modern water masses (Johannesen et al., 1994). The paired $\delta^{18}O$ and $\delta^{13}C$ measurements from the present study show a water mass signature during Bølling-Allerød that closely resembles modern day isotope pairs from the Eastern Fram Strait (Fig 9) (Volkmann & Mensch, 2001).

5.2.2 Period: 12,850 to 11,650 cal yr B.P. (Younger Dryas)

During Younger Dryas the planktic foraminiferal fauna assemblage is dominated by *N. pachyderma* indicating cold polar sea surface conditions (Fig 8). TOC and $CaCO_3$ values reach their minima during this period indicating, in conjunction with low planktic fluxes, lowered primary production in the water column (Fig 4). Especially cold conditions are recorded in the later part of Younger Dryas at ca. 12,100 to 11,800 cal yr B.P. During this period the lowest foraminiferal fluxes were recorded and an insufficient specimen concentration prevented stable isotope analysis (Fig 5, 6). Furthermore, the lowest IRD concentrations may indicate more sustained, perhaps perennial sea ice cover (e.g. Wollenburg et al., 2004). The recorded $SST_{Mg/Ca}$ values, averaging ca. 3°C, are only slightly lower than during Bølling/Allerød. Approximately the same average temperature was recorded by the $SST_{Transfer}$ (Fig 8). The $\delta^{13}C$ values recorded during Younger Dryas show increased values at ca. 12,800 cal yr B.P., in addition to just before and after the almost barren interval at ca. 12,100 to 11,800 cal yr B.P. The high $\delta^{13}C$ values most likely reflect periods of increased mixing of the upper water column (Fig 6). Prior to ca. 12,100 cal yr B.P. the $\delta^{18}O$ values steadily increase indicating declining temperatures and/or increasing salinities (Fig 6). After 11,800 cal yr B.P. following the almost barren interval the $\delta^{18}O$ values decreased and values remained low at 11,800 to 11,500 cal yr B.P. (Fig 6). The absence of planktic foraminifera followed by low $\delta^{18}O$ values would suggest increased influence from less saline waters which could denote an eastward extension of Polar Waters from the EGC. Apart from the high SSS calculated immediately after the barren interval a marked salinity decrease from ca. 35 to 34 at 11,750 to 11,600 cal yr B.P. tentatively supports this interpretation (Fig 8). The $SST_{Mg/Ca}$ and the high SSSs (average ca. 35) indicate that cool Atlantic Water dominated the subsurface water mass during most of Younger Dryas (Fig 8). This is supported by the paired $\delta^{18}O$ and $\delta^{13}C$ values that during Younger Dryas mainly resembled present day values in the eastern Fram Strait (Fig 9). However, some paired $\delta^{18}O$ and $\delta^{13}C$ values tend toward an isotopic signal that more resembles values found in modern Polar and Arctic Front areas indicating that that subsurface water mass was less stable during Younger Dryas than during the preceding Bølling/Allerød (Fig 9).

5.2.3 Period: 11,650 to 10,500 cal yr B.P. (Earliest Holocene)

The continued dominance of the polar *N. pachyderma* and low planktic fluxes show that cold surface conditions prevailed during the earliest part of the Holocene (Fig 5). The primary production was slightly higher than during the Younger Dryas indicated by slightly elevated planktic fluxes (Fig 4), while increased $\delta^{13}C$ indicate better ventilation (Fig 6). The $SST_{Mg/Ca}$

shows an average of 3.5°C which is similar to values recorded during Bølling/Allerød, while salinity values show a declining trend with average values slightly lower (ca. 34.5) than in the preceding periods (Fig 8). Despite the lower salinities, the paired isotopic $\delta^{18}O$ and $\delta^{13}C$ signal are still similar to modern Atlantic Water composition in the Eastern Fram Strait. However, the paired isotopic values during the earliest Holocene exhibit somewhat lower overall variability and are generally slightly lower in $\delta^{18}O$ and higher in $\delta^{13}C$ (Fig 9). The trend goes towards present day values recorded in Polar Water from the Nordic Seas, which may indicate more frequent episodic eastward extension of Polar Waters from the EGC during the earliest Holocene than during Younger Dryas (Fig 9). Generally high and fluctuating $\delta^{18}O$ values are observed during the earliest Holocene indicating rapid changes of temperature and/or salinity (Fig 7). A marked excursion towards heavier $\delta^{18}O$ values at ca. 11,500 to 11,300 cal yr B.P. probably depicts a period of especially cold conditions (Fig 6). However, the relatively low resolution of the $SST_{Mg/Ca}$ dataset inhibits confirmation of a cooling and the faunal distribution pattern does not depict any significant changes (Fig 5, 7). This brief period is followed by decreasing $\delta^{18}O$ values toward the top of the period which indicates increasing temperatures and/or decreasing salinities. This is tentatively supported by SSS values that show a declining trend while both $SST_{Mg/Ca}$ and $SST_{Transfer}$ show minute average increases (Fig 6, 8). The amount of sand and IRD rose during the earliest Holocene (Fig 4). This apparent increased iceberg melting activity in the area might have been a contributing factor to the continued moderately low planktic fluxes (Fig 8). At ca. 11,000 cal yr B.P. a distinct IRD peak, the maximum value of the record, might indicate a marked iceberg or sea ice rafting event (Fig 4).

5.2.4. Period: 10,500 to 8,600 cal yr B.P. (Early Holocene)

From ca. 10,500 to 10,200 cal yr B.P. the planktic foraminifer flux increased rapidly. Further, the foraminiferal fauna changed to a dominance by the subpolar *T. quinqueloba* (e.g. Johannessen et al., 1994) showing a clear transition from cold to warm sea surface water masses (Fig 5, 8). There is a near absence of IRD and generally low concentration of the sand fraction material in this interval indicating that iceberg transport ceased at 10,500 cal yr B.P (Fig 4). The transition indicates that the Atlantic Water influx towards the north probably had increased, and that Atlantic Water emerged at the surface. At ca. 10,500 to 9,800 cal yr B.P. the sediment record exhibits a high concentration of diatoms (Fig 4) which together with elevated planktic fluxes and increasing $CaCO_3$ values indicate an increased primary production (Fig 4, 5). The clear dominance of *T. quinqueloba* shows that sea ice had

diminished and that the Arctic Front remained in relatively close proximity to the area throughout the period (Johannessen et al., 1994). A pronounced peak in relative percentage and flux of *G. uvula* is observed at ca. 10,000 to 9,300 cal yr B.P. (Fig 5). This opportunistic species tolerates lowered salinities and is found in cold productive surface waters near oceanic fronts (Boltovskoy et al., 1996; Husum and Hald, 2004). Hence, the simultaneous high fluxes of *G. uvula* and *T. quinqueloba* could indicate closer proximity of the Arctic Front (Fig 5). During this period the $\delta^{18}O$ values continued to decrease. Minimum values were reached at ca. 9,800 to 8,800 cal yr B.P. most likely indicating higher temperatures (Fig 6). $SST_{Mg/Ca}$ show 0.5 to 1°C warmer temperatures and salinity is on average 0.5 to 0.75 lower than preceding periods (Fig 8). One distinct excursion towards heavier $\delta^{18}O$ values occurred at ca. 10,000 cal yr B.P. indicating a short lived (<50 yr) cooling (Fig 6). However, this event is not registered by the $SST_{Transfer}$, $SST_{Mg/Ca}$ or SSS reconstructions possibly due to too low resolution of these records (Fig 8). The $SST_{Transfer}$ estimate shows that temperatures at 10 meters water depth rose ca. 5.3°C over a period of ca. 450 years (at 10,700 to 10,250 cal yr B.P.), equivalent to a temperature rise of 0.01°C/yr (Fig 8). The marked $SST_{Transfer}$ increase is not recorded to the same extend by the $SST_{Mg/Ca}$ in the subsurface water mass. However, $SST_{Mg/Ca}$ increased on average 0.5°C after ca. 10,400 cal yr B.P. and confirm a general warming of the upper water mass (Fig 8). The relatively low $\delta^{13}C$ values at ca. 10,300 to 9,000 cal yr B.P. are probably due to less ventilated Atlantic Water in the subsurface water mass rather than decreased primary production in the water column (Fig 6). Similar $\delta^{13}C$ values are observed in the area today (Spielhagen & Erlenkeuser 1994). After ca. 9,000 cal yr B.P. the $\delta^{13}C$ values increase possibly reflecting a more ventilated water mass and/or increased primary productivity (Fig 6), while increased $CaCO_3$ concentrations and continued high planktic fluxes also indicate generally increased primary production. However, the highest $\delta^{13}C$ values recorded at ca. 8,800 cal yr B.P. coincide with a brief period of *N. pachyderma* dominance that combined with decreased planktic fluxes and lower $CaCO_3$ indicates a period of surface cooling and decreased primary production (Fig 4, 6, 8). At ca. 10,300 to 9,000 cal yr B.P. the paired isotopic signal resembles the modern water masses from both the eastern Fram Strait and the North Atlantic (Fig 9). Both these water masses are strongly influenced by Atlantic Water confirming the influence from Atlantic Water in the eastern Fram Strait during the early Holocene. The paired isotopic signal in the youngest part of the record is similar to the isotopic composition of modern water masses found near the Arctic Front in the Nordic Seas indicating that the Arctic Front drew closer to the core site after ca. 9,000 cal yr B.P. (Fig 9).

5.3. Paleoenvironmental correlation

5.3.1. Period: 14,000 to 12,850 cal yr B.P. (Bølling/Allerød interstadial)

The $SST_{Mg/Ca}$, $SST_{Transfer}$ and SSS reconstructions and the paired isotopic signal show that *N. pachyderma* calcified its tests in cool Atlantic Water masses during Bølling-Allerød (Fig 8, 9). The combination of increasing $SST_{Mg/Ca}$ and SSS indicates that the inflowing Atlantic Water became less altered throughout Bølling/Allerød possibly due to increased stratification of the water column and/or progressively decreasing influence from melt water (Fig 6, 8). Low $\delta^{13}C$ values which are indicative of stratification are also recorded further south at ca. 77°N in the Fram Strait (Ebbesen et al., 2007) and at ca. 75°N on the Barents Sea slope (Sarnthein et al., 2003) during this period. The periods of elevated (around 13,600 and 13,100 cal yr B.P.) and lowered IRD concentration (around 13,400 cal yr B.P.) correlate well with cold inter Bølling-Allerød periods recorded in the NGRIP ice core (Rasmussen, S.O. et al., 2006) (Fig 4, 8). The higher IRD concentrations point to increased calving and subsequent transport of and melt out from icebergs or sea ice occurring in periods with cold atmospheric conditions and vice versa. Elevated coarse fraction and IRD in the sediment has previously been reported during Bølling-Allerød on the west Spitsbergen Slope (Rasmussen, T.L. et al., 2007; Ebbesen et al., 2007; Jessen et al., 2010) while lower IRD concentrations were found north of Svalbard under the axis of the Svalbard Branch (Fig 1) which was ascribed to severe sea ice conditions (Koç et al., 2002; Ślubowska-Woldengen et al., 2005). Periods of elevated (around 13,200 cal yr B.P.) and lowered (around 13,700 cal yr B.P.) $SST_{Mg/Ca}$ seem to depict an anti-phase relationship with the NGRIP temperature development (Fig 8) (Rasmussen, S. O. et al., 2006). This anti-phase relationship suggests that colder atmospheric conditions generated prolonged and expanded sea ice cover in the Nordic Seas resulting in submergence of Atlantic Water further south. Thereby the advected Atlantic Water was bound beneath a strongly stratified cold, fresh and sea ice influenced surface water mass. The marine paleo records from Bølling/Allerød show that Atlantic Water dominated in the southern Norwegian Sea along the west coast of Norway (Koç et al., 1993; Klitgaard-Kristensen et al., 2001). Further north the surface waters remained predominantly sea ice covered (Koç et al., 1993). Clear signs of high current speeds during Bølling-Allerød indicate strong meriodional advection of Atlantic Water through the Eastern Fram Strait (Birgel and Hass, 2004). The increased advection of Atlantic Water is however not recognizable in the surface water mass because of prevailing perennial sea ice cover dominating the northern and western Nordic Seas (Koç et al., 1993).

5.3.2. Period: 12,850 to 11,650 cal yr B.P. (Younger Dryas)

The Younger Dryas in the present record depicts cold surface conditions as indicated by the dominance of *N. pachyderma* and low planktic foraminiferal fluxes (Fig 5). The Younger Dryas stadial has been documented in different proxy records in the Arctic Region: ice core records (e.g. Rasmussen, S. O. et al., 2006), terrestrial proxy records (e.g. Landvik et al., 1998), Nordic Sea records (e.g. Koç et al., 1993) and records from the Svalbard archipelago (Ślubowska-Woldengen et al., 2007; 2008). Relatively lowered sand (>63µm) and IRD concentrations during this period (Fig 4) can be interpreted as increased sea ice cover that suppressed iceberg transport, decreased glacier calving on Svalbard and/or surface waters that were too cold to allow melting of icebergs. Low IRD concentrations west and north of Svalbard have previously been linked to prolonged sea ice coverage and diminished iceberg transport during the Younger Dryas (Koç et al., 2002; Wollenburg et al., 2004; Ebbesen et al., 2007; Ślubowska-Woldengen et al., 2007). In the present record SSS, $SST_{Mg/Ca}$ and paired isotopes all identify a cool Atlantic Water mass in the subsurface water column during the Younger Dryas (Fig 8 & 9). Birgel and Hass (2004) found that the Atlantic Water influx to the Arctic Ocean decreased markedly during Younger Dryas while Rasmussen, T. L. et al. (2007) found that some subsurface advection of Atlantic Water continued. The almost foraminiferal-barren interval and subsequent low $\delta^{18}O$ values and decreasing SSS indicate increased freshwater influence in the surface and subsurface water mass at ca. 12,200 to 11,600 cal yr B.P. (Fig 6, 8). Increased freshwater injections from various possible sources and sea ice expansion in the Nordic Seas have previously been identified and linked to hampered meridional overturning circulation during the Younger Dryas (e.g. Broecker et al., 1989; Koç et al., 2003; Hald & Aspeli, 1997, Jennings et al., 2006; Bradley and England, 2008). Birgel and Hass (2004) found that the weakest influx of Atlantic Water to the Arctic Ocean occurred at ca. 12,500 to 12,000 cal yr B.P. which slightly predates the barren interval/low $\delta^{18}O$ event in the present record (Fig 6, 8). The temporal difference might be ascribed to the low dating resolution in the present record (Fig 3). However, at the end of Younger Dryas and into the Preboreal (11,800 to 11,400 cal yr B.P.) generally increasing $SST_{Mg/Ca}$ and SSS estimates (Fig 8) seem to correlate with increased subsurface Atlantic Water advection into the Arctic Ocean (Birgel and Hass, 2004).

5.3.3. Period: 11,650 to 8,600 cal yr B.P. (Early Holocene)

The present study clearly depicts that cold surface water conditions with a low flux foraminiferal fauna dominated by *N. pachyderma* and with continued influence from sea ice and iceberg drifts existed in the earliest Holocene until ca. 10,500 cal yr B.P. (Fig 4, 8). Similar cold sea ice/iceberg influenced surface conditions are recorded both west and north of Svalbard during this period (Ebbesen et al., 2007; Ślubowska-Woldengen et al., 2007). The marked IRD peak observed at ca. 11,000 cal yr B.P. (Fig 4) correlates to a concurrent period of rapid ice retreat on Svalbard and in western Barents Sea (Landvik et al., 1998). The Greenland ice cores record the transition from the cold Younger Dryas to the warm Holocene at 11,650 cal yr B.P. (Rasmussen, S. O. et al., 2006; Walker et al., 2009) (Fig 8) about 1,000 years prior to the transition observed in the present record. The delay observed in the oceanic regime at high latitudes has been attributed to the lingering impact of a cold water and sea ice pool in high Arctic settings (Hald et al., 2007). It has furthermore been connected to high albedo caused by sea ice/snow cover and the related asymmetry of atmospheric and oceanic circulation patterns (e.g. Kaufman et al., 2004). The lack of significant change in $SST_{Mg/Ca}$ and $SST_{Transfer}$ across the Holocene/Younger Dryas transition may also be attributed to continued hampered Atlantic Water influx through the Fram Strait (Birgel and Hass, 2004). The marked heavy $\delta^{18}O$ excursion observed in the present record observed at ca. 11,400 cal yr B.P. (Fig 6) correlates with the Preboreal Oscillation cooling event. This cooling has been observed in various marine proxy records in the Fram Strait, Nordic Seas and in northern Norway (e.g. Björck et al., 1997; Hald and Hagen, 1998; Husum and Hald, 2002; Ślubowska-Woldengen et al., 2005) and in Greenland ice cores (Rasmussen, S. O. et al., 2006, 2007) (Fig 8). Subsequently the $\delta^{18}O$, $SST_{Mg/Ca}$ and SSS exhibit a warming and freshening trend of the subsurface water mass. On the south-western Svalbard slope (76°N) (Rasmussen, T. L. et al., 2007) and on the western Barents Sea shelf (75°N) (Sarnthein et al., 2003) similar trends in $\delta^{18}O$ are observed but with slightly lower values due to either stronger freshwater influence and/or higher overall temperatures. At ca. 10,000 cal yr B.P. another heavy $\delta^{18}O$ excursion is observed that approximately correlates to the so-called 9,95 ka anomaly (presented on the b2k scale) in the Greenland ice cores (Rasmussen, S. O. et al., 2007).

In the present record a marked cold to warm surface water regime shift is observed at ca. 10,500 to 10,200 cal yr to varying extent in most of the studied proxy records. The $SST_{Mg/Ca}$ and $SST_{Transfer}$ estimates show a temperature rise of ca. 0.5°C in the sub surface water mass and ca. 5°C in the surface water mass (at 10 m water depth), respectively (Fig 8). In the Nordic Seas, surface water masses (at 10 m water depth) under the influence of inflowing

Atlantic Water experienced the transition into warm Holocene sea surface conditions at ca. 11,800 cal yr B.P. at ca. 60°N and at ca. 10,500 cal yr B.P. at ca. 77°N as the lingering cold water and sea ice pool gradually diminished (Klitgaard-Kristensen et al., 2001; Ebbesen et al., 2007; Hald et al., 2007). The change observed in the eastern Fram Strait coincides with markedly increased current speeds in the northern Fram Strait indicating stronger Atlantic Water inflow towards the Arctic Ocean after ca. 10,300 cal yr B.P. (Birgel and Hass, 2004). Increased Atlantic Water influence in the eastern Fram Strait is also indicated by paired isotopic values in the present record (Fig 9) and the record at 77°N (Ebbensen et al., 2007). Cessation of iceberg transport, as indicated by absence of IRD in the sediment record after ca. 10,500 cal yr B.P. (Fig 4), occurred almost concurrently all along the west Spitsbergen Slope (Ebbesen et al., 2007; Rasmussen, T. L. et al., 2007; Jessen et al., 2010). This cessation combined with the stronger influence from Atlantic Water resulted in increased primary production in the water column inferred from higher planktic foraminiferal fluxes (Fig 5) (Ebbesen et al., 2007; Rasmussen, T. L. et al., 2007; Ślubowska-Woldengen et al., 2007) and high concentration of diatom frustules in the sediment (Fig 4) (Jessen et al., 2010). Records from the north-eastern Nordic Sea (>71°N), including the present record, located under axis of northward Atlantic Water advection depict a relative increase of *T. quinqueloba* at ca. 11,000 to 10,300 cal yr B.P. and a subsequent sustained dominance for 2.000 to 3.000 years (Hald and Aspeli, 1997; Sarnthein et al., 2003; Ebbesen et al., 2007). This indicates that the Arctic Front, separating the Arctic and Atlantic Water mass, probably was situated close to the west Spitsbergen and Barents Sea slopes during the Early Holocene (Johannessen et al., 1994).

6. Conclusions

A multi proxy study of the late Glacial – early Holocene transition was carried out at the western Svalbard slope at ca. 78˚55 N. The study included planktic foraminiferal fauna distribution, planktic $\delta^{13}C$ and $\delta^{18}O$ stable isotopes and analyses of bulk sediment grain size distribution and carbon. In addition to the more commonly used proxies, the Mg/Ca-ratio temperature proxy is for the first time applied and tested in a high Arctic paleoceanographic setting enabling quantitative reconstructions of sea surface and subsurface temperature and salinity. Mg/Ca-ratios were measured on the planktic foraminiferal species *Neogloboquadrina pachyderma*. The $SST_{Mg/Ca}$ reconstruction shows a relatively stable temperature signal through the Late Glacial-Holocene transition. Both the $SST_{Mg/Ca}$ and SSS reconstructions, the latter calculated on the basis of paired oxygen isotope and Mg/Ca

temperatures, exhibit realistic values that relate to the varying calcification depth of *N. pachyderma*.

From 14,000 to 10,300 cal yr B.P. cold polar sea surface conditions dominated the eastern Fram Strait. Extensive sea ice cover, iceberg transport and low surface temperatures resulted in low foraminiferal fluxes and low primary production. Atlantic Water inflow existed as a subsurface current with temperatures around 3.5°C and salinities around 34.7.

Warm Holocene conditions developed rapidly as the Arctic Front retreated westward at ca. 10,300 cal yr B.P. The surface waters were strongly influenced by Atlantic Water as indicated by high sea surface temperatures around 9°C. There was no influence by sea ice or icebergs and the primary productivity was high. The Arctic Front remained in relative proximity to the core site until 8,600 cal yr B.P. which is shown by the dominance of *Turborotalita quinqueloba*. Subsurface inflow of Atlantic Water continued with a modest average temperature rise of 0.5°C and salinity decrease of 0.4 compared to previous period. After ca. 9,000 cal yr B.P. the Arctic Front reapproached the core site as indicated by the paired oxygen and carbon stable isotope signal.

Acknowledgements

This work has been carried out within the framework of the International Polar Year project "Arctic Natural Climate and Environmental Changes and Human Adaption: From Science to Public Awareness" (SciencePub, IPY # 39) funded by the Research Council of Norway and the Trainee School in Arctic Marine Geology & Geophysics, University of Tromsø. Sediment core and CTD data were collected onboard the R/V "MERIAN S. Merian" during the MSM05/5b expedition led by Dr. Gereon Budeus, Alfred Wegener Institute for Polar and Marine Research, Germany. Jan Petter Holm prepared the area map. Samples were prepared at the laboratory at Department of Geology, University of Tromsø by Trine Dahl. Foraminifer selection and stable isotope analyses at Leibniz Institute of Marine Sciences IFM-GEOMAR were performed by Kristina Pascher and Lulzim Haxhiaj. To these persons and institutions we offer our sincere thanks.

References

Aagaard, K., A. Foldvik, and S. R. Hillman (1987), The West Spitsbergen Current: disposition and water mass transformation, Journal of Geophysical Research, 92, 3778–3784.

Aagaard, K., and E. C. Carmack (1989), The role of sea ice and other fresh water in the Arctic circulation, Journal of Geophysical Research, 94(C14), 14485-14498.

Barker, S., Greaves, M., and Elderfield, H. (2003). A study of cleaning procedures used for foraminiferal Mg/Ca paleothermometry. Geochem. Geophys. Geosyst. 4. Doi. 10.1029/2003gc000559

Bè, A. W. H., and D. S. Tolderlund (1971), Distribution and ecology of living planktonic foraminifera in surface waters of the Atlantic and Indian Oceans, In: Funnel, B.M., Riedel, W.R. (Eds.), The Micropaleontology of Oceans. Cambridge University Press, London, 105–149.

Birgel, D., and H. C. Hass (2004), Oceanic and atmospheric variations during the last deglaciation in the Fram Strait (Arctic Ocean): a coupled high-resolution organic-geochemical and sedimentological study, Quaternary Science Reviews, 23(1-2), 29-47.

Björck, S., M. Rundgren, Ó. Ingólfsson, and S. Funder (1997), The Preboreal oscillation around the Nordic Seas: terrestrial and lacustrine responses, Journal of Quaternary Science, 12(6), 455-465.

Blindheim, J., and F. Rey (2004), Water-mass formation and distribution in the Nordic Seas during the 1990s, ICES Journal of Marine Science, 61(5), 846-863.

Boltovskoy, E., D. Boltovskoy, N. Correa & F. Brandini (1996) Planktic foraminifera from the southwestern Atlantic (30°–60°S): species-specific patterns in the upper 50 m. Marine Micropaleontology, 28, 53–72.

Boyle, E. A., and Keigwin, L. D. (1985). Comparison of Atlantic and Pacific paleochemical records for the last 215,000 years: changes in deep ocean circulation and chemical inventories. Earth and Planetary Science Letters 76, 135-150.

Boyle, E. A., and Rosenthal, Y. (1996). Chemical hydrography of the South Atlantic during the Last Glacial Maximum: Cd and d13C, in The South Atlantic: Present and Past Circulation. edited by G. Wefer et al. Springer-Verlag, New York, 423 –443.

Bourke, R. H., A. M. Weigel, and R. G. Paquette (1988), The Westward Turning Branch of the West Spitsbergen Current, J. Geophys. Res., 93, 14065-14077.

Bradley, R. S. & J. H. England (2008) The Younger Dryas and the Sea of Ancient Ice. *Quaternary Research*, 70**,** 1-10.

Broecker, W. S., J. P. Kennett, B. P. Flower, J. T. Teller, S. Trumbore, G. Bonani & W. Wolfli (1989) Routing of meltwater from the Laurentide Ice Sheet during the Younger Dryas cold episode. Nature 341. 318–321

Carstens, J. H., and G. Wefer (1992), Recent distribution of planktonic foraminifera in the Nansen Basin, Arctic Ocean, Deep-sea research. Part A, Oceanographic research papers, 39(2A), 507-524.

Craig, H. and L. I. Gordon (1965), Deuterium and oxygen 18 variations in the ocean and marine atmosphere. In proc. Stable Isotopes in Oceanographic Studies and Paleotemperatures, Spoleto, Italy. edited by E. Tongiogi, 9-130.

Darling KF, Kucera M, Kroon D and Wade CM (2006) A resolution forthe coiling direction paradox in Neogloboquadrina pachyderma. Paleoceanography 21: PA2011, doi:10.1029/2005PA001189.

Ebbesen, H., M. Hald, and T. H. Eplet (2007), Late glacial and early Holocene climatic oscillations on the western Svalbard margin, European Arctic, *Quarternary Science Reviews, 26*(15-16), 1999-2011.

Elderfield, H., and Ganssen, G. M. (2000). Past temperature and d^{18}O of surface ocean waters inferred from foraminiferal Mg/Ca ratios. Nature 405, 442–445.

Elderfield, H., Vautravers, M., and Cooper, M. (2002). The relationship between shell size and Mg/Ca, Sr/Ca, $\delta^{18}O$, and $\delta^{13}C$ of species of planktonic foraminifera. Geochem. Geophys. Geosyst. 3(8). Doi:10.1029/2001gc000194

Fairbanks, R. G. (1989). A 17,000-year glacio-eustatic sea level record : influence of glacial melting rates on the Younger Dryas event and deep-ocean circulation. Nature (London) 342, 637-642.

Hald, M. & R. Aspeli (1997) Rapid climatic shifts of the nothern Norwegian Sea during the last deglaciation and the Holocene. Boreas, 26, 15-28.

Hald, M., and S. Hagen (1998), Early preboreal cooling in the Nordic Sea region triggered by meltwater Geology 26, 615-618.

Hald, M., Andersson, C., Ebbesen, H., Jansen, E., Klitgaard-Kristensen, D., Risebrobakken, B., Salomonsen, G. R., Sejrup, H. P., Sarnthein, M., and Telford, R. (2007). Variations in temperature and extent of Atlantic Water in the northern North Atlantic during the Holocene. Quaternary Science Reviews 26, 3423-3440.

Hopkins, T. S. (1991), The GIN Sea--A synthesis of its physical oceanography and literature review 1972-1985, Earth-Science Reviews, 30(3-4), 175-318.

Hughen, K. A., Baillie, M. G. L., Bard, E., Beck, J. W., Bertrand, C. J. H., Blackwell, P. G., Buck, C. E., Burr, G. S., Cutler, K. B., Damon, P. E., Edwards, R. L., Fairbanks, R. G., Friedrich, M., Guilderson, T. P., Kromer, B., McCormac, G., Manning, S., Ramsey, C. B., Reimer, P. J., Reimer, R. W., Remmele, S., Southon, J. R., Stuiver, M., Talamo, S., Taylor, F. W., van der Plicht, J., and Weyhenmeyer, C. E. (2004). Marine04 marine radiocarbon age calibration, 0-26 cal kyr BP. Radiocarbon 46, 1059-1086.

Husum, K., and M. Hald (2002), Early Holocene cooling events in Malangenfjord and the adjoining shelf, north-east Norwegian Sea, Polar Research, 21(2), 267-274.

Husum, K., and M. Hald (2004), Modern Foraminiferal Distribution in the Subarctic Malangen Fjord and adjoining Shelf, Northern Norway, Journal of Foraminiferal Research, 34(1), 34-48.

IPCC (2007) Climate Change 2007: The physical science basis. Summary for policymakers, intergovernmental panel on climate change. Fourth Assessment Report, Geneva, IPCC Secretariat**,** 1–18.

Jennings, A. E., M. Hald, M. Smith & J. T. Andrews (2006) Freshwater forcing from the Greenland Ice Sheet during the Younger Dryas: evidence from southeastern Greenland shelf cores. *Quaternary Science Reviews,* 25**,** 282-298.

Jessen, S. P., T. L. Rasmussen, T. Nielsen, and A. Solheim (2010), A new Late Weichselian and Holocene marine chronology for the western Svalbard slope 30,000-0 cal years BP, Quaternary Science Reviews, 29(9-10), 1301-1312.

Johannessen, T., E. Jansen, A. Flatøy, and A. C. Ravalo (1994), The relationship between surface water masses, oceanographic fronts and paleoclimatic proxies in surface sediments of the Greenland, Iceland and Norwegian Seas., NATO ASI series I, 17, 61-85.

Jonkers, L., Brummer, G.-J. A., Peeters, F. J. C., van Aken, H. M., and De Jong, M. F. (2010). Seasonal stratification, shell flux, and oxygen isotope dynamics of left-coiling *N. pachyderma* and *T. quinqueloba* in the western subpolar North Atlantic. Paleoceanography 25, PA2204. Doi: 10.1029/2009pa001849

Juggins, S. (2002). C2 1.3 version: http://www.staff.ncl.ac.uk/stephen.juggins.

Katz, M. E., B. S. Cramer, A. Franzese, B. Honisch, K. G. Miller, Y. Rosenthal & J. D. Wright (2010) Traditional and emerging geochemical proxies in foraminifera. *Journal of Foraminiferal Research,* 40**,** 165-192.

Kaufman, D.S., Ager, T.A., Anderson, N.J., Anderson, P.M., Andrews, J.T., Bartlein, P.J., Brubaker, L.B., Coats, L.L., Cwynar, L.C., Duvall, M.L., Dyke, A.S., Edwards, M.E., Eisner, W.R., Gajewski, K., Geirsdottir, A., Hu, F.S., Jennings, A.E., Kaplan, M.R., Kerwin, M.W., Lozhkin, A.V., MacDonald, G.M., Miller, G.H., Mock, C.J., Oswald, W.W., Otto-Bliesner, B.L., Porinchu, D.F., Ruhland, K., Smol, J.P., Steig, E.J., and Wolfe, B.B., 2004, Holocene thermal maximum in the western Arctic (0-180°W), Quaternary Science Reviews, 23, 529-560.

Klitgaard-Kristensen, D., H. P. Sejrup, and H. Haflidason (2001), The last 18 kyr fluctuations in Norwegian Sea surface conditions and implicationsfor the magnitude of climatic change, evidence from the northern North Sea, Paleoceanography, 16, 455–467.

Knies, J., M. Hald, H. Ebbesen, U. Mann & C. Vogt (2003) A deglacial—middle Holocene record of biogenic sedimentation and paleoproductivity changes from the northern Norwegian continental shelf. *Paleoceanography,* 18**,** 1096, doi:10.1029/2002PA000872

Koç, N., E. Jansen, and H. Haflidason (1993), Paleoceanographic reconstructions of surface ocean conditions in the Greenland, Iceland and Norwegian seas through the last 14 ka based on diatoms, Quaternary Science Reviews, 12(2), 115-140.

Koç, N., D. Klitgaard-Kristensen, K. Hasle, C. F. Forsberg, and A. Solheim (2002), Late glacial palaeoceanography of Hinlopen Strait, northern Svalbard, Polar Research, 21(2), 307-314.

Kozdon, R., Eisenhauer, A., Weinelt, M., Meland, M. Y., and Nürnberg, D. (2009). Reassessing Mg/Ca temperature calibrations of *Neogloboquadrina pachyderma* (sinistral) using paired δ44/40Ca and Mg/Ca measurements. Geochemistry Geophysics Geosystems 10. Doi:10.1029/2008GC002169

Landvik, J. Y., S. Bondevik, A. Elverhoi, W. Fjeldskaar, J. Mangerud, O. Salvigsen, M. J. Siegert, J.-I. Svendsen, and T. O. Vorren (1998), The last glacial maximum of Svalbard and the Barents sea area: ice sheet extent and configuration, Quaternary Science Reviews, 17(1-3), 43-75.

Loeng, H., V. Ozhigin, and B. Ådlandsvik (1997), Water fluxes through the Barents Sea, ICES Journal of Marine Science, 54(3), 310-317.

Mangerud, J., and Gulliksen, S. (1975). Apparent radiocarbon ages of Recent marine shells from Norway, Spitsbergen, and Arctic Canada. Quaternary Research 5, 263-273.

Mangerud, J., Bondevik, S., Gulliksen, S., Hufthammer, A. K., and Høisæter, T. (2006). Marine14 C reservoir ages for 19th century whales and molluscs from the North Atlantic. Quaternary Science Reviews 25, 3228-3245.

Manley, T. O. (1995), Branching of Atlantic Water within the Greenland-Spitsbergen passage: An estimate of recirculation, J. Geophys. Res., 100, 20627-20634.

Marchitto, T. M. (2006). Precise multielemental ratios in small foraminiferal samples determined by sector field ICP-MS. Geochem. Geophys. Geosyst. 7. Doi: 10.1029/2005gc001018

Marnela, M., B. Rudels, K. A. Olsson, L. G. Anderson, E. Jeansson, D. J. Torres, M.-J. Messias, J. H. Swift, and A. J. Watson (2008), Transports of Nordic Seas water masses and excess SF6 through Fram Strait to the Arctic Ocean, Progress In Oceanography, 78(1), 1-11.

Meredith, M., K. Heywood, P. Dennis, L. Goldson, R. White, E. Fahrbach, U. Schauer, and S. Østerhus (2001), Freshwater fluxes through the Western Fram Strait, Geophys. Res. Lett., 28(8), 1615–1618, doi:10.1029/2000GL011992.

Mosby, H. (1962), Water, salt and heat balance of the North Polar Sea and the Norwegian Sea, Geophys. Norv., 24(11), 289– 313.

Nyland, B. F., E. Jansen, H. Elderfield & C. Andersson (2006) *Neogloboquadrina pachyderma* (dex. and sin.) Mg/Ca and d18O records from the Norwegian Sea. Geochem. Geophys. Geosyst., 7, Q10P17. doi: 10.1029/2005gc001055

Pflaumann, U., J. Duprat, C. Pujol & L. D. Labeyrie (1996) SIMMAX: A Modern Analog Technique to Deduce Atlantic Sea Surface Temperatures from Planktonic Foraminifera in Deep-Sea Sediments. *Paleoceanography*, 11**,** 15-35.

Pflaumann, U., Sarnthein, M., Chapman, M., d'Abreu, L., Funnell, B., Huels, M., Kiefer, T., Maslin, M., Schulz, H., Swallow, J., van Kreveld, S., Vautravers, M., Vogelsang, E., and Weinelt, M. (2003). Glacial North Atlantic: Sea-surface conditions-reconstructed by GLAMAP 2000. Paleoceanography 18(3). 1065, doi:10.1029/2002PA000774

Rasmussen, S. O., Andersen, K. K., Svensson, A. M., Steffensen, J. P., Vinther, B. M., Clausen, H. B., Siggaard-Andersen, M.-L., Johnsen, S. J., Larsen, L. B., Dahl-Jensen, D., Bigler, R. R., M. , Fischer, H., Goto-Azuma, K., Hansson, M. E., and Ruth, U. (2006). A new Greenland ice core chronology for the last glacial termination. Journal of Geophysical Research 111, 16 pp, doi:10.1029/2005JD006079.

Rasmussen, S. O., Vinther, B. M., Clausen, H. B., and Andersen, K. K. (2007). Early Holocene climate oscillations recorded in three Greenland ice cores. Quaternary Science Reviews 26, 1907-1914.

Rasmussen, T. L., E. Thomsen, M. A. Slubowska, S. Jessen, A. Solheim, and N. Koc (2007), Paleoceanographic evolution of the SW Svalbard margin (76^0N) since 20,000 ^{14}C yr BP, Quaternary Research, 67(1), 100-114.

Reimer, P. J., Baillie, M. G. L., Bard, E., Bayliss, A., Beck, J. W., Bertrand, C. J. H., Blackwell, P. G., Buck, C. E., Burr, G. S., Cutler, K. B., Damon, P. E., Edwards, R. L., Fairbanks, R. G., Friedrich, M., Guilderson, T. P., Hogg, A. G., Hughen, K. A., Kromer, B., McCormac, F. G., Manning, S. W., Ramsey, C. B., Reimer, R. W., Remmele, S., Southon, J. R., Stuiver, M., Talamo, S., Taylor, F. W., van der Plicht, J., and Weyhenmeyer, C. E. (2004). IntCal04 Terrestrial radiocarbon age calibration, 26 - 0 ka BP. Radiocarbon 46, 1029-1058.

Reimer, P. J., Baillie, M. G. L., Bard, E., Bayliss, A., Beck, J. W., Blackwell, P. G., Bronk Ramsey, C., Buck, C. E., Burr, G. S., Edwards, R. L., Friedrich, M., Grootes, P. M., Guilderson, T. P., Hajdas, I., Heaton, T. J., Hogg, A. G., Hughen, K. A., Kaiser, K. F., Kromer, B., McCormac, F. G., Manning, S. W., Reimer, R. W., Richards, D. A., Southon, J. R., Talamo, S., Turney, C. S. M., van der Plicht, J., and Weyhenmeyer, C. E. (2009). IntCal09 and Marine09 Radiocarbon Age Calibration Curves, 0–50,000 Years cal BP. Radiocarbon 51, 1111–1150.

Rudels, B., J. F. H, and D. Quadfasel (1999), The Arctic Circumpolar Boundary Current, Deep Sea Research Part II: Topical Studies in Oceanography, 46, 1023-1062.

Rudels, B., G. Björk, J. Nilsson, P. Winsor, I. Lake, and C. Nohr (2005), The interaction between waters from the Arctic Ocean and the Nordic Seas north of Fram Strait and along the East Greenland Current: results from the Arctic Ocean-02 Oden expedition, Journal of Marine Systems, 55(1-2), 1-30.

Sarnthein, M., S. Van Kreveld, H. Erlenkeuser, P. M. Grootes, M. Kucera, U. Pflaumann & M. Schulz (2003) Centennial-to-millennial-scale periodicities of Holocene climate and sediment injections off the western Barents shelf, 75°N. Boreas, 32, 447 - 461.

Schauer, U., H. Loeng, B. Rudels, V. K. Ozhigin & W. Dieck (2002) Atlantic Water flow through the Barents and Kara Seas. *Deep Sea Research Part I: Oceanographic Research Papers,* 49**,** 2281-2298.

Schauer, U., E. Fahrbach, S. Osterhus, and G. Rohardt (2004), Arctic warming through the Fram Strait: Oceanic heat transport from 3 years of measurements, Journal of Geophysical Research, 109, C06026, doi:06010.01029/02003JC001823.

Schauer, U., and A. Beszczynska-Möller (2009), Problems with estimation and interpretation of oceanic heat transport - conceptual remarks for the case of Fram Strait in the Arctic Ocean, Ocean Sci., 5(4), 487-494.

Shackleton, N. J. (1974). Attainment ofisotopic equilibrium between ocean water and the benthonic foraminifera genus *Uvigerina*: isotopic changes in the ocean during the last glacial. Centre National de la Recherche Scientifique Colleagues Internationeau 219, 203-209.

Simstich, J., Sarnthein, M., and Erlenkeuser, H. (2003). Paired delta O-18 signals of *Neogloboquadrina pachyderma* (s) and *Turborotalita quinqueloba* show thermal stratification structure in Nordic Seas. Marine Micropaleontology 48, 107-125.

Skogseth, R., P. M. Haugan, and M. Jakobsson (2005), Watermass transformations in Storfjorden, Continental Shelf Research, 25(5-6), 667-695.

Ślubowska-Woldengen, M., N. Koç, T. L. Rasmussen, and D. Klitgaard-Kristensen (2005), Changes in the flow of Atlantic water into the Arctic Ocean since the last deglaciation: Evidence from the northern Svalbard continental margin, 80°N, *Paleoceanography*, *20*, PA001141. doi: 10.1029/2005PA001141

Slubowska-Woldengen, M., T. L. Rasmussen, N. Koç, D. Klitgaard-Kristensen, F. Nilsen, and A. Solheim (2007), Advection of Atlantic Water to the western and northern Svalbard shelf since 17,500 cal yr BP, *Quaternary Science Reviews*, *26*(3-4), 463-478.

Ślubowska-Woldengen, M., N. Koç, T. L. Rasmussen, D. Klitgaard-Kristensen, M. Hald, and A. E. Jennings (2008), Time-slice reconstructions of ocean circulation changes on the continental shelf in the Nordic and Barents Seas during the last 16,000 cal yr B.P., Quaternary Science Reviews, 27(15-16), 1476-1492.

Spielhagen, R. F. & H. Erlenkeuser (1994) Stable oxygen and carbon isotopes in planktic foraminifers from Arctic Ocean surface sediments: Reflection of the low salinity surface water layer. Marine Geology, 119**,** 227-250.

Spielhagen, R. F., K. Werner, S. A. Sørensen, K. Zamelczyk, E. Kandiano, G. Budeus, K. Husum, T. M. Marchitto & M. Hald (2011) Enhanced Modern Heat Transfer to the Arctic by Warm Atlantic Water. *SCIENCE,* 331**,** 450-453.

Steffensen, J. P., Andersen, K. K., Bigler, M., Clausen, H. B., Dahl-Jensen, D., Fischer, H., Goto-Azuma, K., Hansson, M., Johnsen, S. J., Jouzel, J., Masson-Delmotte, V., Popp, T., Rasmussen, S. O., Rothlisberger, R., Ruth, U., Stauffer, B., Siggaard-Andersen, M.-L., Sveinbjornsdottir, A. E., Svensson, A., and White, J. W. C. (2008). High-Resolution Greenland Ice Core Data Show Abrupt Climate Change Happens in Few Years. Science 321, 680-684.

Stuiver, M., Reimer, P. J., and Reimer, R. W. 2005. CALIB 6.0. [WWW program and documentation].

Swift, J. H. (1986), The Arctic waters. In: Hurdle, B.G. (Ed.), The Nordic Seas, Springer, New York, 129–153.

Telford, R. J., Andersson, C., Birks, H. J. B., and Juggins, S. (2004). Biases in the estimation of transfer function prediction errors. Paleoceanography 19. Doi 10.1029/2004pa001072

Telford, R. J., and Birks, H. J. B. (2005). The secret assumption of transfer functions: problems with spatial autocorrelation in evaluating model performance. Quaternary Science Reviews 24, 2173-2179.

Volkmann, R. (2000), Planktic foreminifers in the outer Laptev Sea and the Fram Strait - Modern distribution and ecology, Journal of Foraminiferal Research, 30(3), 157-176.

Volkmann, R. & M. Mensch (2001) Stable isotope composition ($\delta^{18}O$, $\delta^{13}C$) of living planktic foraminifers in the outer Laptev Sea and the Fram Strait. Marine Micropaleontology, 42, 163-188.

Walczowski, W., J. Piechura, R. Osinski, and P. Wieczorek (2005), The West Spitsbergen Current volume and heat transport from synoptic observations in summer, Deep Sea Research Part I: Oceanographic Research Papers, 52(8), 1374-1391.

Walker, M., Johnsen, S., Rasmussen, S. O., Popp, T., Steffensen, J.-P., Gibbard, P., Hoek, W., Lowe, J., Andrews, J., Björck, S., C. Cwynar, L., Hughen, K., Kershaw, P., Kromer, B., Litt, T., J. Lowe, D., Nakagawa, T., Newnham, R., and Schwander, J. (2009). Formal definition and dating of the GSSP (Global Stratotype Section and Point) for the base of the Holocene using the Greenland NGRIP ice core, and selected auxiliary records. Journal of Quaternary Science 24, 3-17.

Winkelmann, D., and J. Knies (2005), Recent distribution and accumulation of organic carbon on the continental margin west off Spitsbergen, Geochem. Geophys. Geosyst., 6(9), Q09012. Doi. 10.1029/2005gc000916

Wollenburg, J. E., J. Knies, and A. Mackensen (2004), High-resolution paleoproductivity fluctuations during the past 24 kyr as indicated by benthic foraminifera in the marginal Arctic Ocean, Palaeogeography, Palaeoclimatology, Palaeoecology, 204, 209-238.

Woodgate, R. A., E. Fahrbach, and G. Rohardt (1999), Structure and transports of the East Greenland Current at 75°N from moored current meters, J. Geophys. Res., 104(C8), 18059-18072.

Östlund, H. G., H. Craig, W. S. Broecker, and D. Spencer (1987), GEOSECS Atlantic, Pacific, and Indian ocean expeditions. Shorebased data and graphics, GEOSECS Atlas Series, US Govt Printing Office, Washington DC, 7, 1-200.

Figure captions

Table 1. Radiocarbon dates and calibrations from core MSM5/5-712. The radiocarbon dates were performed by the Leibniz-Laboratory for Radiometric Dating and Isotope Research, Kiel, Germany (KIA) and at Poznań Radiocarbon Laboratory, Poland (Poz). A reservoir age correction of 400 years with an additional reservoir correction (ΔR) of 151±51 was used.

Figure 1. (A) Map of northern North Atlantic and adjoining seas showing the core location, major currents systems, oceanic fronts sea ice limits modified from Mosby (1968), Hopkins (1991) and Marnela et al. (2008). (B) Bathymetric map of the Fram Strait showing the core site. AO is Arctic Ocean, BS is Barents Sea.

Figure 2. Temperature and salinity profile from the core site measured in August 2007.

Figure 3. Age model and bulk sediment accumulation rate of core MSM05/5-712-2. The age model is developed by linear interpolation between the calibrated radiocarbon dated levels.

Figure 4. (A) Selected grain sizes (weight %) >63 µm and <63 µm and lithological units; (B) Grain sizes (weight %) >1 mm (IRD); (C) Total organic carbon (TOC) (wt.%); (D) Total carbon (TC) (wt.%) and (E) Calcium carbonate ($CaCO_3$) (wt.%). All data are expressed versus calibrated age and depth. Shaded area = Diatom-rich layer. Chronostratigraphical zones follow Rasmussen, S. O. et al. (2007), Steffensen et al. (2008) and Walker et al. (2009). Diamonds on X-axis indicate radiocarbon dated levels.

Figure 5. The five most abundant planktic foraminiferal species plotted against age and core depth are shown. The black lines show relative planktic foraminiferal species distribution. The grey area indicates the flux of individual species and total flux of planktic foraminifera on logarithmic scale (grey area). In addition, summer SST reconstructions based on planktic foraminiferal transfer functions are also shown. Three statistical techniques have been applied: maximum likelihood (ML; thick line with circles), modern analogue technique (MAT; dashed line with crosses) and weighted averaging partial least square (WAPLS; thin line with triangles). For chronostratigraphical zones see captions Fig 4.

Figure 6. Planktic stable isotope measurements (A) $\delta^{13}C$, (B) $\delta^{18}O$ with 5-point running mean (black line). Filled circles show the average reproducibility of isotopic measurements. For chronostratigraphical zones see captions Fig 4.

Figure 7. Trace metal concentrations (mmol/mol) plotted against age and depth. (A) Left: Mg/Ca. The thin line shows the raw data, and the thick line is the five-point running mean. The dashed line shows the linear regression ($Y = -2*10^{-5} X + 1.05$). The crosses mark omitted data points. The filled circle shows the average reproducibility of sample splits (±0.049 mmol/mol). Right: Reconstructed sub $SST_{Mg/Ca}$; (B) Mn/Ca and (C) Fe/Ca concentrations. The dashed lines show the threshold level of possible contamination (Barker et al., 2003). For chronostratigraphical zones see captions Fig 4.

Figure 8. (A) Reconstructed paleo sea surface temperatures ($SST_{Isotope}$ (five-point running mean), $SST_{Mg/Ca}$ five-point running mean) and $SST_{Transfer}$), (B) paleo $\delta^{18}O_{water}$ (‰) and (C) paleo sea surface salinities (SSS) plotted against age and depth. Also shown is (D) relative planktic foraminiferal species distribution of *N. pachyderma*, *T. quinqueloba*, and other species (See Fig 5 for details) and (E) oxygen stable oxygen isotopes ($\delta^{18}O$) record obtained from the NGRIP ice core. For chronostratigraphical zones see captions Fig 4.

Figure 9. Stable isotope values of $\delta^{18}O$ and $\delta^{13}C$ plotted against each other grouped in three time intervals; (A) 14,000 to 12,850 cal yr B.P.; (B) 12,850 to 10,300 cal yr B.P. and (C) 10,300 to 8,600 cal yr B.P. The $\delta^{18}O$ values were corrected for the ice volume

effect according to Fairbanks (1989). In addition, the paired isotopic value representing modern surface sediment values from the Nordic Seas (Johannessen et al., 1994) and eastern Fram Strait (Volkmann & Mensch, 2001) are shown.

Table 1

Lab. code	Depth range (cm)	Material	^{14}C age	Calibrated age ± 2σ	2 σ max cal. age (cal. age intercepts) 2 σ min cal. age	Reservoir age (R=400 + ΔR)	$\delta^{13}C$(‰)
Poz-30723	214-215	*N. pachyderma*	8362±45	cal. BP 8749 ±209	cal. BP 8540 (8749) 8958	551±51	-0.6 ± 0.4
KIA 37423	280-281	*N. pachyderma*	9220±50	cal. BP 9797±252	cal. BP 9551 (9797) 10042	551±51	-2.99 ± 0.35
Poz-30725	322-323	*N. pachyderma*	9580±47	cal. BP 10310 ±158	cal. BP 10152 (10310) 10468	551±51	-2.6 ± 0.1
Poz-30726	428-431	*N. pachyderma*	12358±63	cal. BP 13629±197	cal. BP 13432 (13629) 13826	551±51	-1.1 ± 0.1

Figure 1

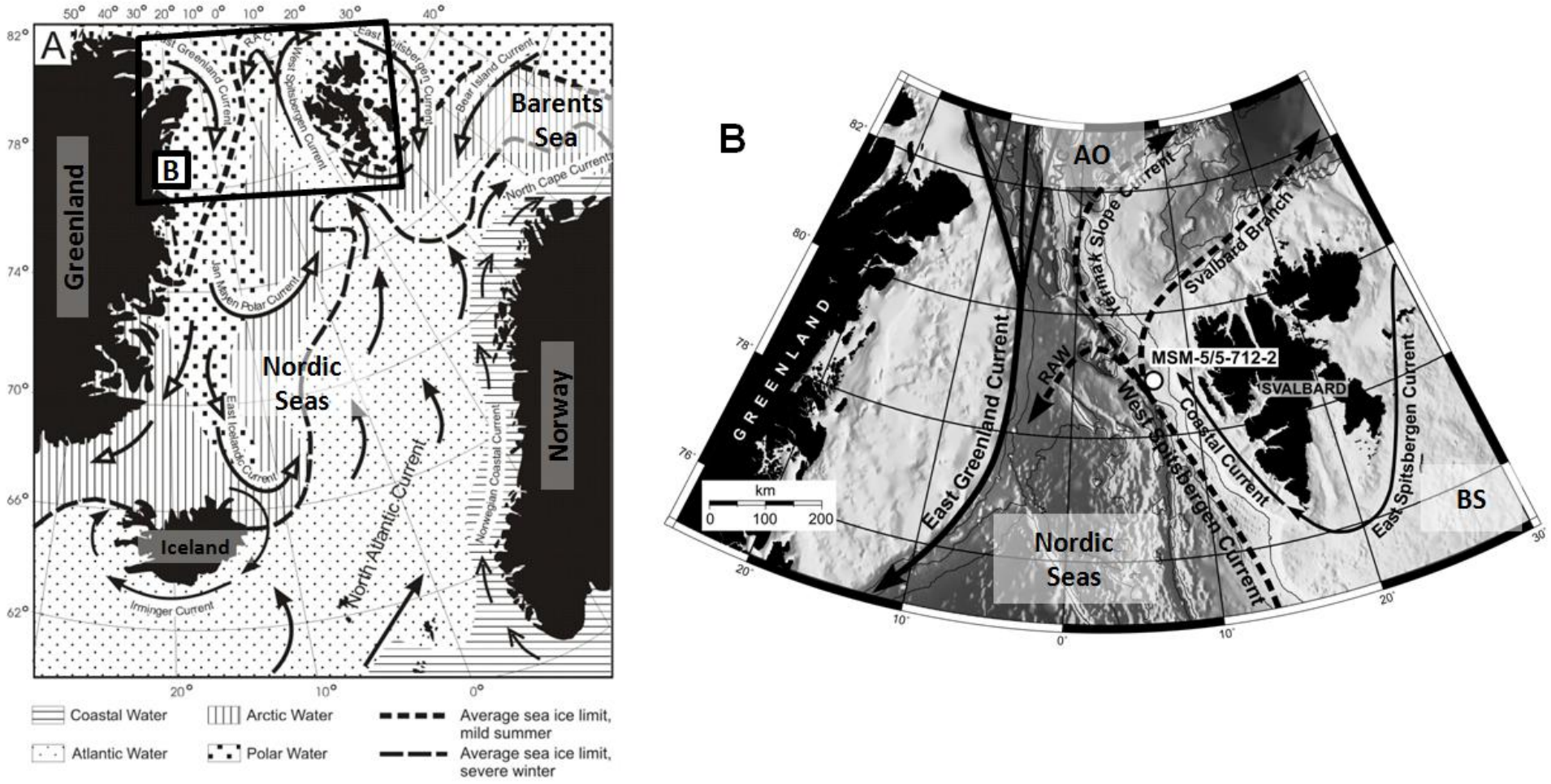
A
B
Greenland
Iceland
Barents Sea
Nordic Seas
Norway
East Greenland Current
West Spitsbergen Current
Bear Island Current
North Cape Current
Jan Mayen Polar Current
East Icelandic Current
North Atlantic Current
Norwegian Coastal Current
Irminger Current
Coastal Water
Atlantic Water
Arctic Water
Polar Water
Average sea ice limit, mild summer
Average sea ice limit, severe winter
B
AO
Fram Strait
Polar Slope Current
Svalbard Branch
RAW
MSM-5/5-712-2
SVALBARD
West Spitsbergen Current
Coastal Current
East Spitsbergen Current
BS
km
0 100 200

Figure 2

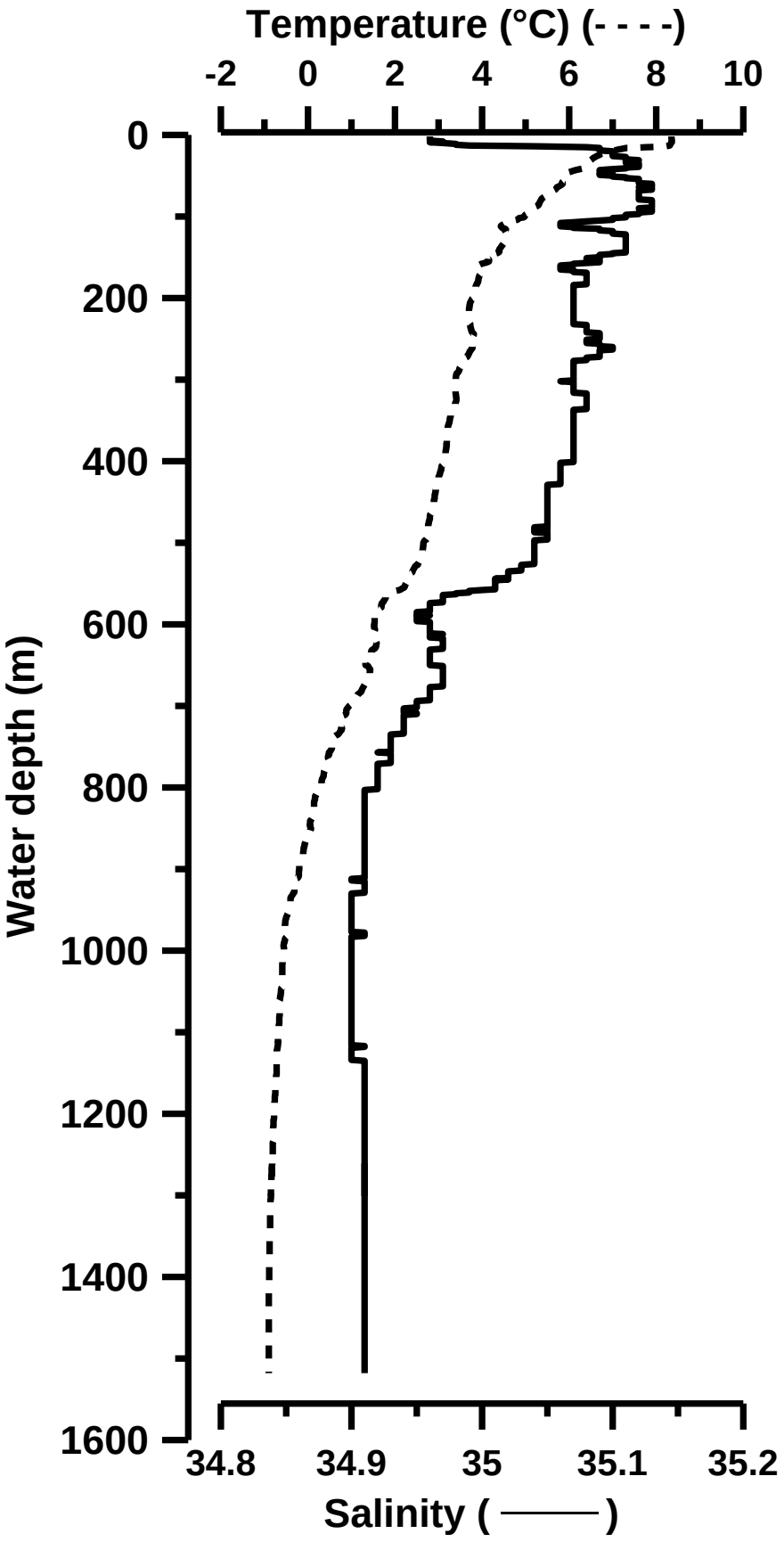
Temperature (°C) (- - - -)
-2
0
2
4
6
8
10
0
200
400
600
800
1000
1200
1400
1600
Water depth (m)
34.8
34.9
35
35.1
35.2
Salinity (———)

Figure 3

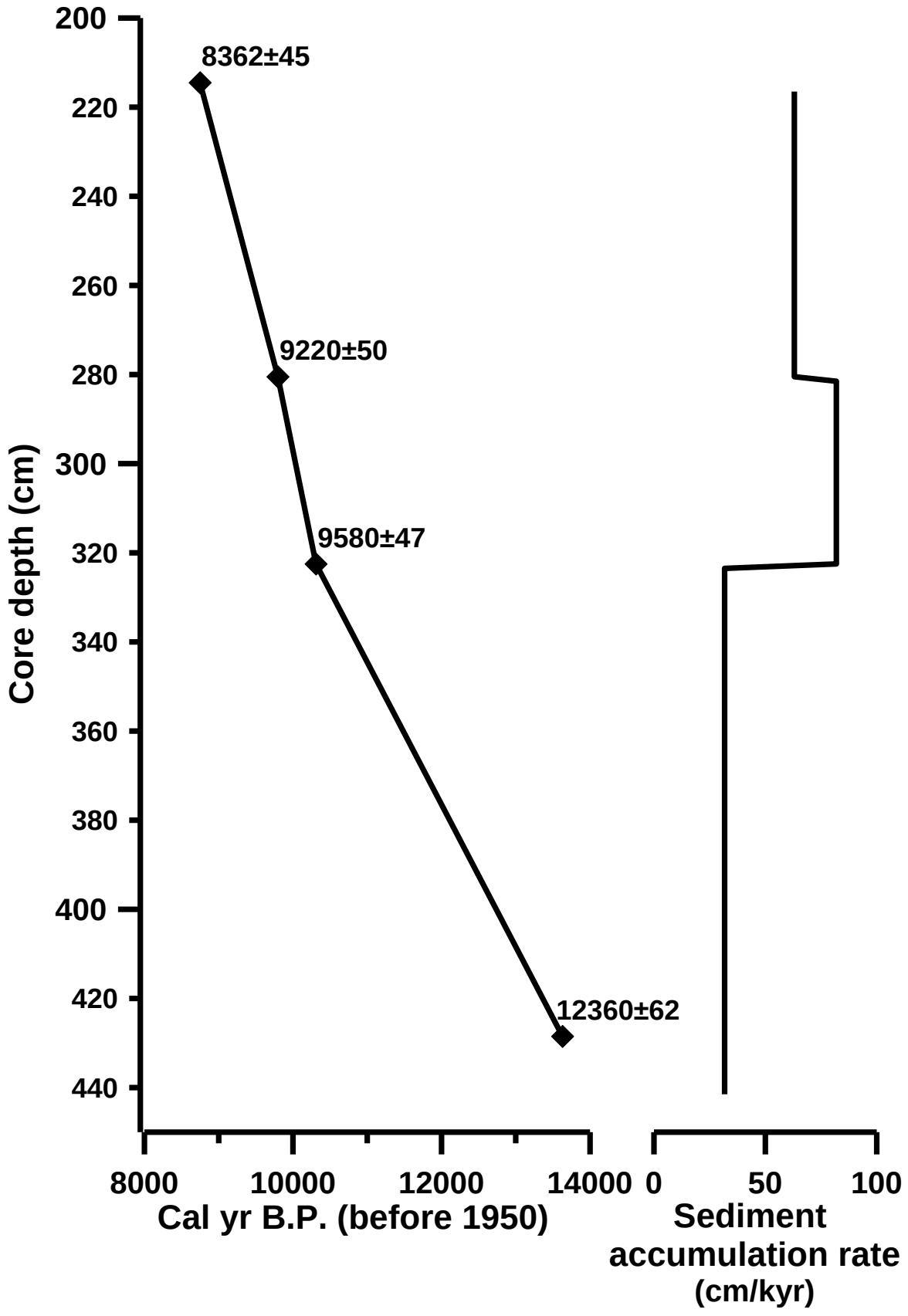
200
220
240
260
280
300
320
340
360
380
400
420
440
Core depth (cm)
8362±45
9220±50
9580±47
12360±62
8000
10000
12000
14000
Cal yr B.P. (before 1950)
0
50
100
Sediment accumulation rate (cm/kyr)

Figure 4

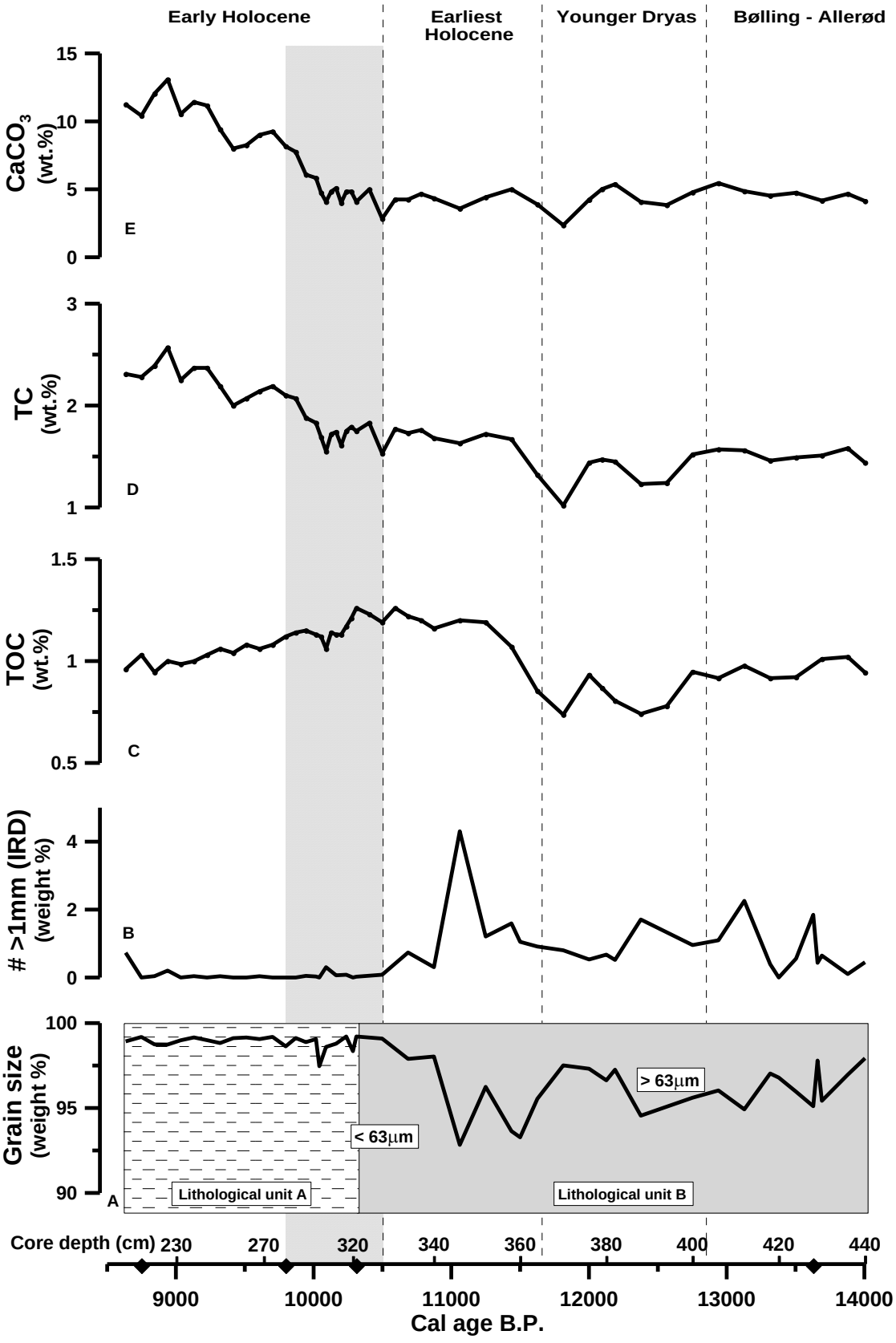
Early Holocene
Earliest Holocene
Younger Dryas
Bølling - Allerød
CaCO3 (wt.%)
E
TC (wt.%)
D
TOC (wt.%)
C
>1mm (IRD) (weight %)
B
Grain size (weight %)
< 63μm
> 63μm
Lithological unit A
Lithological unit B
A
Core depth (cm)
Cal age B.P.

Figure 5

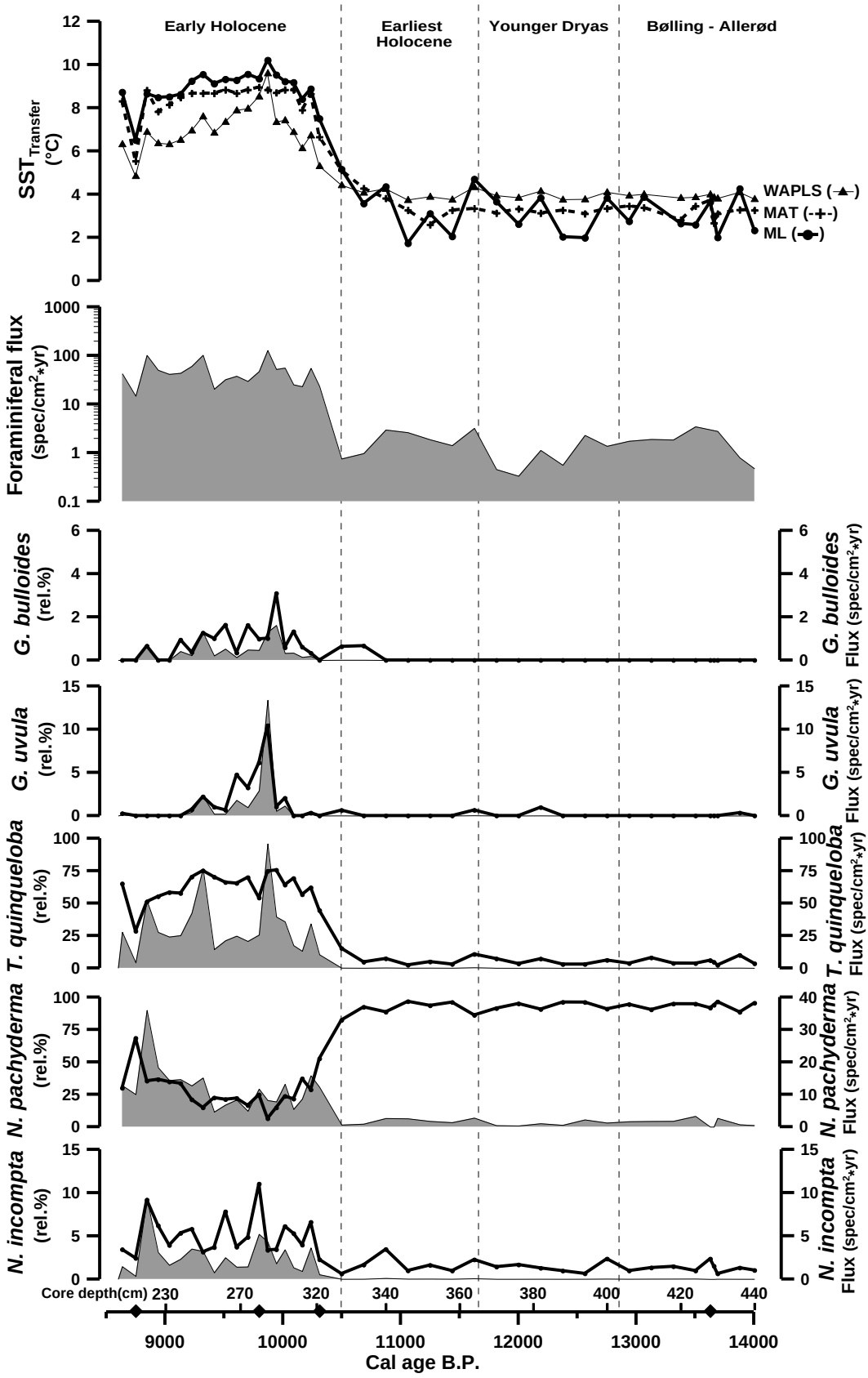
Early Holocene
Earliest Holocene
Younger Dryas
Bølling - Allerød
SST Transfer (°C)
WAPLS (-▲-)
MAT (-+-)
ML (-●-)
Foraminiferal flux (spec/cm²*yr)
G. bulloides (rel.%)
G. bulloides Flux (spec/cm²*yr)
G. uvula (rel.%)
G. uvula Flux (spec/cm²*yr)
T. quinqueloba (rel.%)
T. quinqueloba Flux (spec/cm²*yr)
N. pachyderma (rel.%)
N. pachyderma Flux (spec/cm²*yr)
N. incompta (rel.%)
N. incompta Flux (spec/cm²*yr)
Core depth(cm) 230 270 320 340 360 380 400 420 440
9000 10000 11000 12000 13000 14000
Cal age B.P.

Figure 6

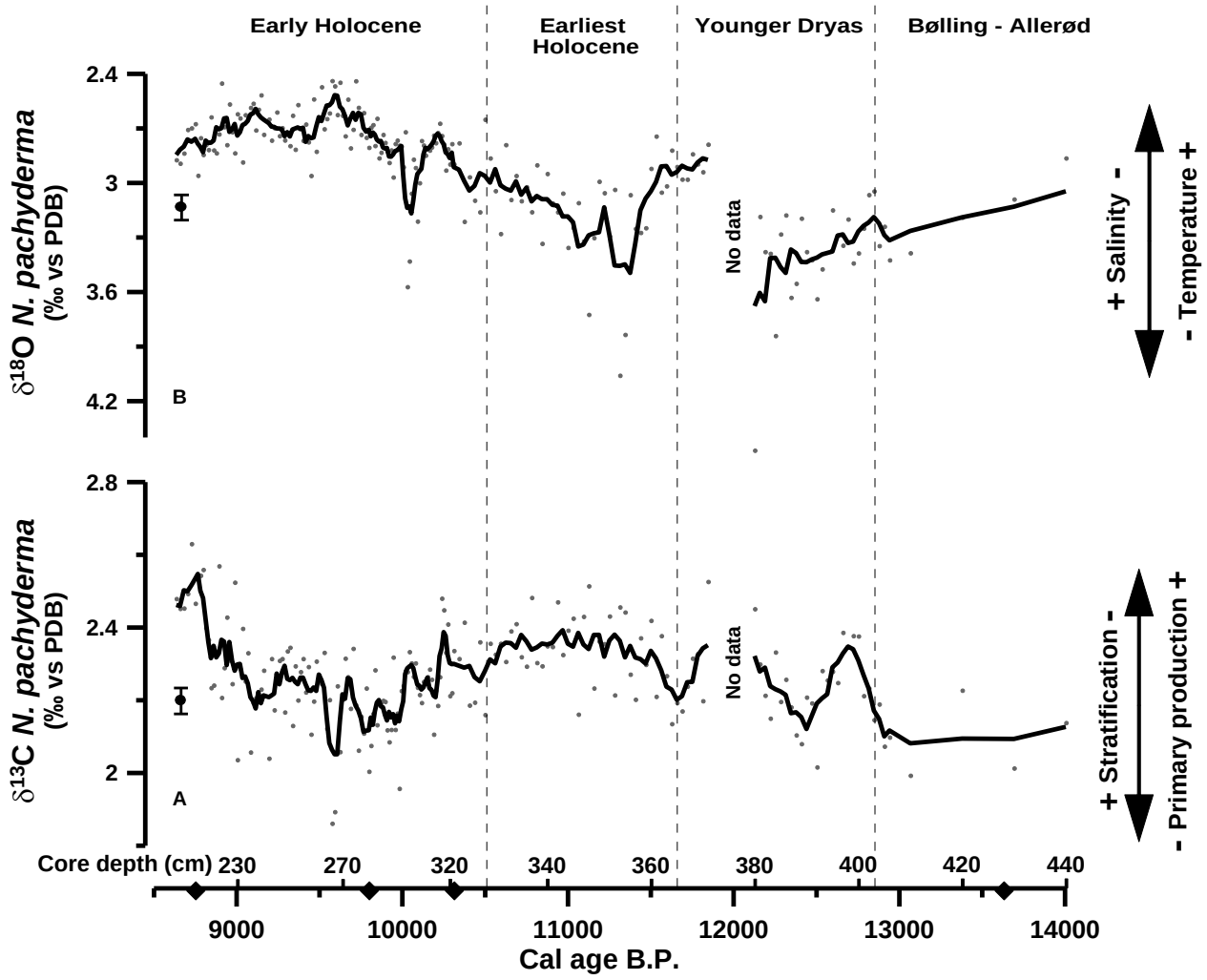
Early Holocene
Earliest Holocene
Younger Dryas
Bølling - Allerød
2.4
3
3.6
4.2
δ18O N. pachyderma (‰ vs PDB)
B
No data
+ Salinity -
- Temperature +
2.8
2.4
2
δ13C N. pachyderma (‰ vs PDB)
A
No data
+ Stratification -
- Primary production +
Core depth (cm) 230 270 320 340 360 380 400 420 440
9000 10000 11000 12000 13000 14000
Cal age B.P.

Figure 7

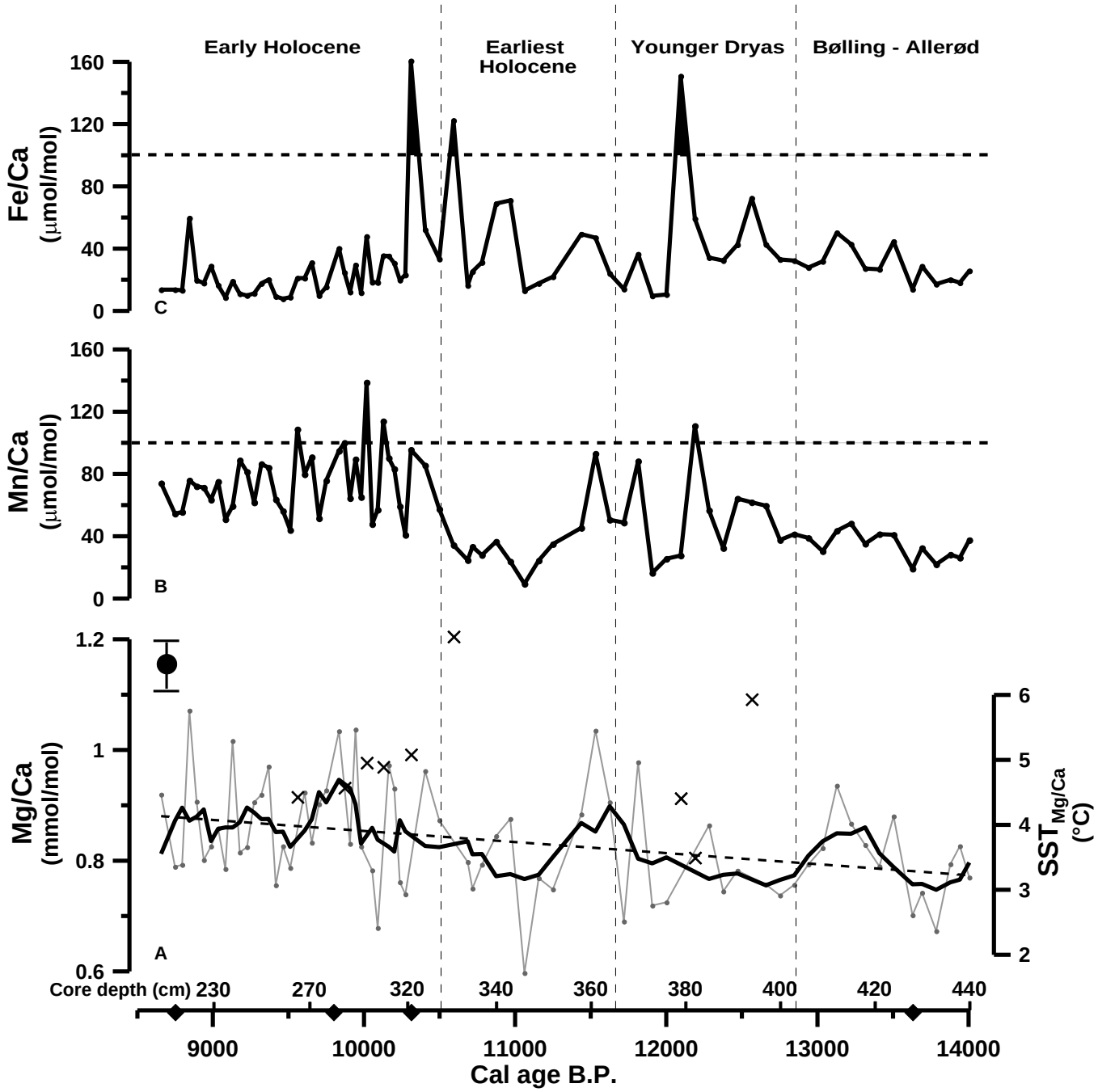
Early Holocene
Earliest Holocene
Younger Dryas
Bølling - Allerød
Fe/Ca (μmol/mol)
Mn/Ca (μmol/mol)
Mg/Ca (mmol/mol)
SST Mg/Ca (°C)
A
B
C
Core depth (cm)
Cal age B.P.

Figure 8

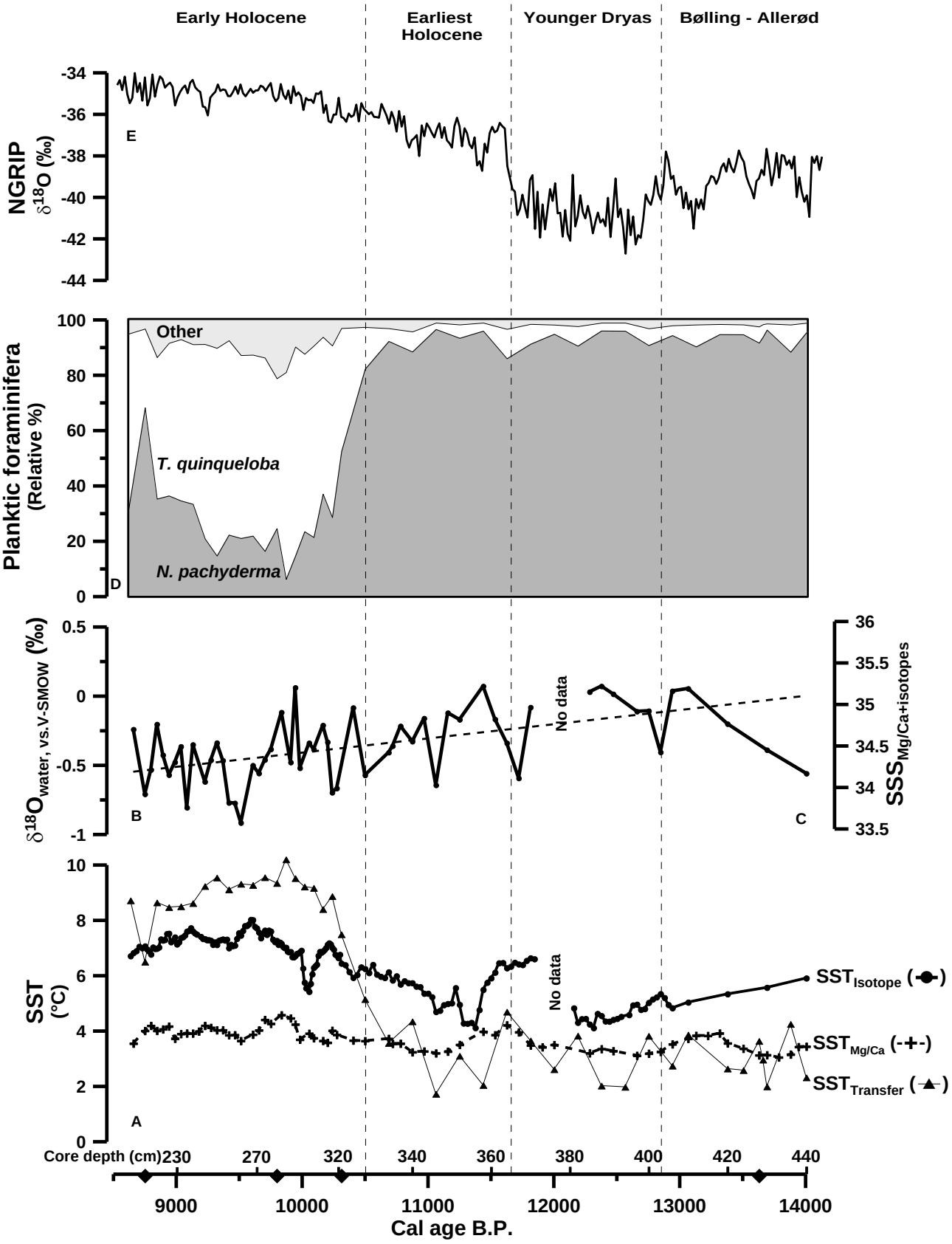
Early Holocene
Earliest Holocene
Younger Dryas
Bølling - Allerød
NGRIP
δ18O (‰)
-34
-36
-38
-40
-42
-44
E
Planktic foraminifera
(Relative %)
Other
T. quinqueloba
N. pachyderma
100
80
60
40
20
0
D
δ18Owater, vs.V-SMOW (‰)
0.5
0
-0.5
-1
B
No data
C
SSSMg/Ca+isotopes
36
35.5
35
34.5
34
33.5
SST
(°C)
10
8
6
4
2
0
A
No data
SSTIsotope (-●-)
SSTMg/Ca (-+-)
SSTTransfer (-▲-)
Core depth (cm)
230
270
320
340
360
380
400
420
440
9000
10000
11000
12000
13000
14000
Cal age B.P.

Figure 9

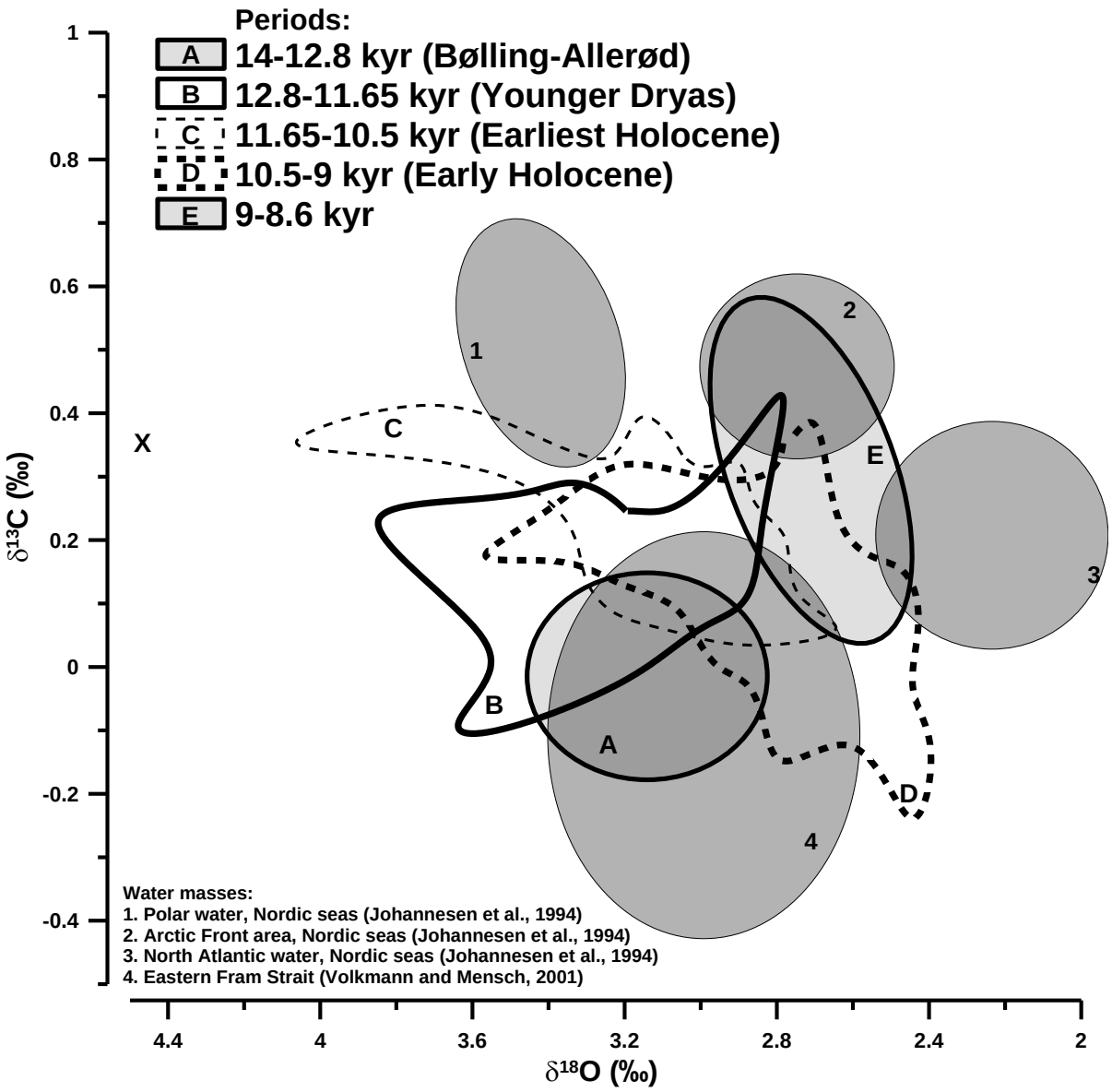
Periods:
A 14-12.8 kyr (Bølling-Allerød)
B 12.8-11.65 kyr (Younger Dryas)
C 11.65-10.5 kyr (Earliest Holocene)
D 10.5-9 kyr (Early Holocene)
E 9-8.6 kyr
X
1
2
3
4
A
B
C
D
E
Water masses:
1. Polar water, Nordic seas (Johannesen et al., 1994)
2. Arctic Front area, Nordic seas (Johannesen et al., 1994)
3. North Atlantic water, Nordic seas (Johannesen et al., 1994)
4. Eastern Fram Strait (Volkmann and Mensch, 2001)
δ13C (‰)
δ18O (‰)
1
0.8
0.6
0.4
0.2
0
-0.2
-0.4
4.4
4
3.6
3.2
2.8
2.4
2